© 2018. Published by The Company of Biologists Ltd | Journal of Cell Science (2018) 131, jcs226241. doi:10.1242/jcs.226241

RESEARCH ARTICLE

Alpha-synuclein fibrils recruit TBK1 and OPTN to lysosomal damage sites and induce autophagy in microglial cells

Claudio Bussi[1,*], Javier M. Peralta Ramos[1], Daniela S. Arroyo[1], Jose I. Gallea[2], Paolo Ronchi[3], Androniki Kolovou[3], Ji M. Wang[4], Oliver Florey[5], Maria S. Celej[2], Yannick Schwab[3,6], Nicholas T. Ktistakis[5] and Pablo Iribarren[1,‡]

ABSTRACT

Autophagic dysfunction and protein aggregation have been linked to several neurodegenerative disorders, but the exact mechanisms and causal connections are not clear and most previous work was done in neurons and not in microglial cells. Here, we report that exogenous fibrillary, but not monomeric, alpha-synuclein (AS, also known as SNCA) induces autophagy in microglial cells. We extensively studied the dynamics of this response using both live-cell imaging and correlative light-electron microscopy (CLEM), and found that it correlates with lysosomal damage and is characterised by the recruitment of the selective autophagy-associated proteins TANK-binding kinase 1 (TBK1) and optineurin (OPTN) to ubiquitylated lysosomes. In addition, we observed that LC3 (MAP1LC3B) recruitment to damaged lysosomes was dependent on TBK1 activity. In these fibrillar AS-treated cells, autophagy inhibition impairs mitochondrial function and leads to microglial cell death. Our results suggest that microglial autophagy is induced in response to lysosomal damage caused by persistent accumulation of AS fibrils. Importantly, triggering of the autophagic response appears to be an attempt at lysosomal quality control and not for engulfment of fibrillar AS.

This article has an associated First Person interview with the first author of the paper.

KEY WORDS: Alpha-synuclein, Autophagy, Microglia, Lysosomes, Cell death

INTRODUCTION

Neurodegenerative diseases are characterised by common cellular and molecular mechanisms, including protein aggregation and inclusion body formation, which result in toxicity and neuronal cell death (Lumkwana et al., 2017).

Autophagy dysfunction in the central nervous system (CNS) has been shown to induce neurodegeneration even in the absence of any disease-associated mutant proteins. Mice deficient for *Atg5* (autophagy-related 5) develop progressive deficits in motor function that are accompanied by the accumulation of cytoplasmic inclusion bodies in neurons (Hara et al., 2006). Additionally, mice lacking *Atg7* specifically in the CNS showed behavioural defects, a reduction in coordinated movement and massive neuronal loss in the cerebral and cerebellar cortices (Komatsu et al., 2006).

Although latest developments reveal a crucial role for the autophagy pathway in neurodegenerative diseases (Frake et al., 2015), the precise mechanisms underlying these processes are poorly understood. Furthermore, most of the existing literature related to autophagy in the CNS focuses on neurons, with the effects of the autophagy pathway and its modulation on microglial cells remaining poorly characterised. Microglia are resident macrophage cells in the CNS and have multiple functions such as phagocytosis, production of growth factors and cytokines, and antigen presentation. The major function of microglia is to maintain homeostasis and normal function of the CNS, both during development and in response to CNS injury (Ransohoff, 2016).

Canonical autophagy starts with the assembly of a pre-initiation complex consisting of ULK1, FIP200 and ATG13, which in turn leads to activation of the VPS34–Beclin-1 PI3K complex, and then formation and extension of a double-membraned autophagosome around cellular contents by the lipidation of the autophagic protein light chain 3 (MAP1LC3B, LC3 hereafter), through the action of two ubiquitin-like conjugation systems. ULK1 is subject to regulatory phosphorylation by mTOR and AMPK, and this provides a means for the control of autophagy in response to nutrient status (Ktistakis and Tooze, 2016).

Lipidated LC3 was once thought to unambiguously distinguish autophagosomes from other cellular membranes. However, in recent years, a non-canonical autophagy mechanism was reported in the literature that depends on direct LC3 association with single limiting-membrane vacuoles and is able to deliver the luminal content towards lysosomal degradation (Martinez et al., 2011). This unconventional pathway is known as LC3-associated phagocytosis (LAP), and is involved in the maturation of single-membrane phagosomes and subsequent killing of ingested pathogens by phagocytes. LAP is initiated following recognition of pathogens by pattern-recognition receptors and leads to the recruitment of LC3 into the phagosomal membrane (Martinez et al., 2015).

Numerous autophagic receptors have been reported to control the delivery of specific cargoes to the lysosomes through autophagy. Wild et al. (2011) characterised an autophagic adaptor, optineurin (OPTN), as a key component of pathogen-induced autophagy. They also showed that this process was regulated by the activation of TANK-binding kinase 1 (TBK1), which binds and phosphorylates OPTN on Ser177, leading to enhanced binding to Atg8 proteins such as LC3 (Wild et al., 2011). Recently, it has also been shown

[1]Centro de Investigaciones en Bioquímica Clínica e Inmunología (CIBICI-CONICET), Departamento de Bioquímica Clínica, Facultad de Ciencias Químicas, Universidad Nacional de Córdoba, Córdoba 5000, Argentina. [2]Centro de Investigaciones en Química Biológica de Córdoba (CIQUIBIC-CONICET), Departamento de Química Biológica Ranwel Caputto, Facultad de Ciencias Químicas, Universidad Nacional de Córdoba, Córdoba 5000, Argentina. [3]EMBL, Electron Microscopy Core Facility, Heidelberg 69117, Germany. [4]Laboratory of Molecular Immunoregulation, Cancer and Inflammation Program, Center for Cancer Research, National Cancer Institute at Frederick, Frederick, MD 20982, USA. [5]Babraham Institute, Signalling Programme, Cambridge CB22 3AT, UK. [6]EMBL, Cell Biology and Biophysics Unit, Heidelberg 69117, Germany.
*Present address: The Francis Crick Institute, London NW1 1AT, UK.

[‡]Author for correspondence (piribarr@fcq.unc.edu.ar)

C.B., 0000-0002-9396-9042; P.I., 0000-0002-5679-4386

Received 8 October 2018; Accepted 9 October 2018

Journal of Cell Science (2018) 131, jcs226241. doi:10.1242/jcs.226241

that the TBK1–OPTN axis targets damaged mitochondria for degradation via PINK1/parkin-mediated mitophagy (Moore and Holzbaur, 2016). As an upstream binding partner for the autophagy receptor, TBK1 phosphorylates OPTN on damaged mitochondria, leading to the formation of a TBK1–OPTN complex. Inhibition and depletion of TBK1 or OPTN blocks the efficient turnover of depolarised mitochondria. Interestingly, mutations of OPTN and TBK1 are both associated with neurodegenerative diseases including amyotrophic lateral sclerosis (ALS), Huntington's disease, Alzheimer's disease, Parkinson's disease, Creutzfeld–Jacob disease and Pick's disease (Korac et al., 2013; Li et al., 2016). However, the mechanistic basis underlying the specific interaction between OPTN and TBK1 in these disorders is still elusive.

Parkinson's disease (PD) is a late-onset neurodegenerative disorder that mainly affects the motor system. Neuronal loss in the substantia nigra, which causes striatal dopamine deficiency, and Lewy bodies, intracellular inclusions containing aggregates of alpha-synuclein (SNCA, AS hereafter), are the neuropathological hallmarks of PD. AS may contribute to PD pathogenesis by distinct mechanisms, but novel evidence suggests that its aberrant fibril conformations are the toxic species that mediate disruption of cellular homeostasis and neuronal death, through effects on various intracellular targets including synaptic function (Peelaerts et al., 2015). In addition, recent reports indicate that AS induces mitochondrial and lysosomal dysfunction and alters vesicular trafficking in PD, which may lead to AS accumulation (Di Maio et al., 2016; Mazzulli et al., 2016). In this scenario, the autophagy pathway plays a critical role as the main mechanism responsible for abnormal protein and organelle degradation (Osellame and Duchen, 2014).

Furthermore, secreted AS may exert deleterious effects on neighbouring neuronal and glial cells, including seeding of aggregations, thus contributing to disease propagation. A pivotal aspect of this cell-to-cell propagation is the ability of these aggregates to enter target cells and reach the cytosol where they induce further pathological protein aggregation.

Even though several reports have indicated that neuronal-released amyloid aggregates can be internalised by glial cells (Asai et al., 2015; Kim et al., 2013; Loria et al., 2017), the mechanisms by which these toxic aggregates escape the endosomal compartment to access the cytosol and encounter the pool of naïve soluble proteins, promoting further protein aggregation, remains largely unknown. Understanding this mechanism of vesicular escape is essential to revealing the mechanisms underlying cell-to-cell propagation of amyloid pathology (Flavin et al., 2017).

Recent research suggests a complex role for microglia not only in PD but in other disorders involving AS aggregation, such as multiple system atrophy (Sanchez-Guajardo et al., 2015). In addition, the novel concepts of AS being released in exosomes and taken up by neighbouring cells, and their importance in disease progression, positions microglia as the main cell that can efficiently clear and handle AS (Chang et al., 2013; Longhena et al., 2017).

Although substantial progress has been made in unravelling the role and regulation of the autophagy machinery, its dysfunction in pathology as well as its dynamic changes in the disease progression remains largely unclear (Lumkwana et al., 2017). Further characterisation of autophagy dynamics not only in neuronal but also in glial cells, in combination with analysis of the ultrastructural details of the several organelles and mechanisms involved in specific subtypes of autophagy, may contribute to the development of novel therapeutic approaches in PD and other neurodegenerative disorders.

In this report we investigated for the first time the effect of monomeric and fibrillar AS on the autophagy activity of microglial cells. We observed that only fibrillar AS induces autophagy in microglial cells and that activation of the autophagy pathway is concomitant to lysosomal rupture. We provide the first evidence showing both the recruitment of TBK1 and OPTN to ubiquitylated lysosomes, and the related autophagy dynamics, through the use of high-resolution and live-cell CLEM in AS-stimulated microglial cells. Moreover, we found that LC3 recruitment to damaged lysosomes was dependent on TBK1 activity and that autophagy inhibition induced mitochondrial and lysosomal quality impairment, which led to microglial cell death after fibrillar AS stimulation. Collectively, our results suggest that microglial autophagy is triggered as a rescue mechanism to restore lysosomal quality control and not as an immediate response to AS internalisation.

RESULTS

Fibrillar, but not monomeric, AS induces autophagy in microglial cells

We first analysed the effect of different AS aggregation states on autophagy induction in microglial cells. We stimulated murine microglial cell line BV2 and murine primary microglial cells with both exogenous fibrillar and monomeric AS at different time points. Based on a previous report from our group, we selected 1 µM as the experimental protein concentration as no significant toxicity is observed either in BV2 or primary microglial cells after long-term cell culture (Bussi et al., 2017). Interestingly, we observed using immunofluorescence visualisation (Fig. 1A) that fibrillar, but not monomeric, AS increased the punctate localisation of LC3. In addition, this response increased substantially after 12 h of stimulation (Fig. 1A).

We next aimed to determine the subcellular localisation of fibrillar AS after cellular internalisation and its distribution in comparison to the autophagy marker LC3. We stimulated BV2 cells stably expressing GFP–LC3 (BV2 GFP–LC3) with Alexa Fluor 594-labelled AS fibrils for 12 h, then, BV2 cells were stained for lysosomal-associated membrane protein 1 (LAMP-1). We found, using confocal microscopy and enhanced visualisation by means of 3D cell surface rendering approaches, that AS fibrils were confined to lysosomes and LC3 vesicles were distributed around them (Fig. 1B–E). Furthermore, we obtained similar results in primary microglial cells immunostained with anti-LC3 antibody (Fig. 1F–I). In order to confirm lysosomal localisation for AS fibrils, we analysed the co-localisation between the lysosomal-specific enzyme N-acetylgalactosamine-6-sulfatase (GALNS) and fibrillar AS in primary microglial cells. Accordingly, these results showed a high degree of co-localisation between both labels (Fig. S1A).

In parallel experiments, we studied the autophagic response using immunoblotting. Initiation of autophagy causes the conversion of LC3-I to LC3-II via the addition of a phosphatidylethanolamine (PE) group to the C-terminus. We evaluated the conversion of LC3-I (non-lipidated form with lower electrophoretic mobility) to LC3B-II (LC3 form C-terminally lipidated by PE, displaying higher electrophoretic mobility). In agreement with our previous results, we found an increase in the intensity of the LC3B-II band relative to the intensity of β-actin band after fibrillary, but not monomeric, AS stimulation (Fig. 1J). When bafilomycin A1 (BAF) was added to fibrillar AS (hereafter fAS)-stimulated cells, we observed an increase in the relative levels of LC3-II in comparison with AS stimulation alone, indicating that fAS induces autophagy in microglial cells and it does not simply block autophagosome degradation (Fig. 1J). Overall, these results show that fAS has predominantly lysosomal localisation after cellular internalisation

Journal of Cell Science (2018) 131, jcs226241. doi:10.1242/jcs.226241

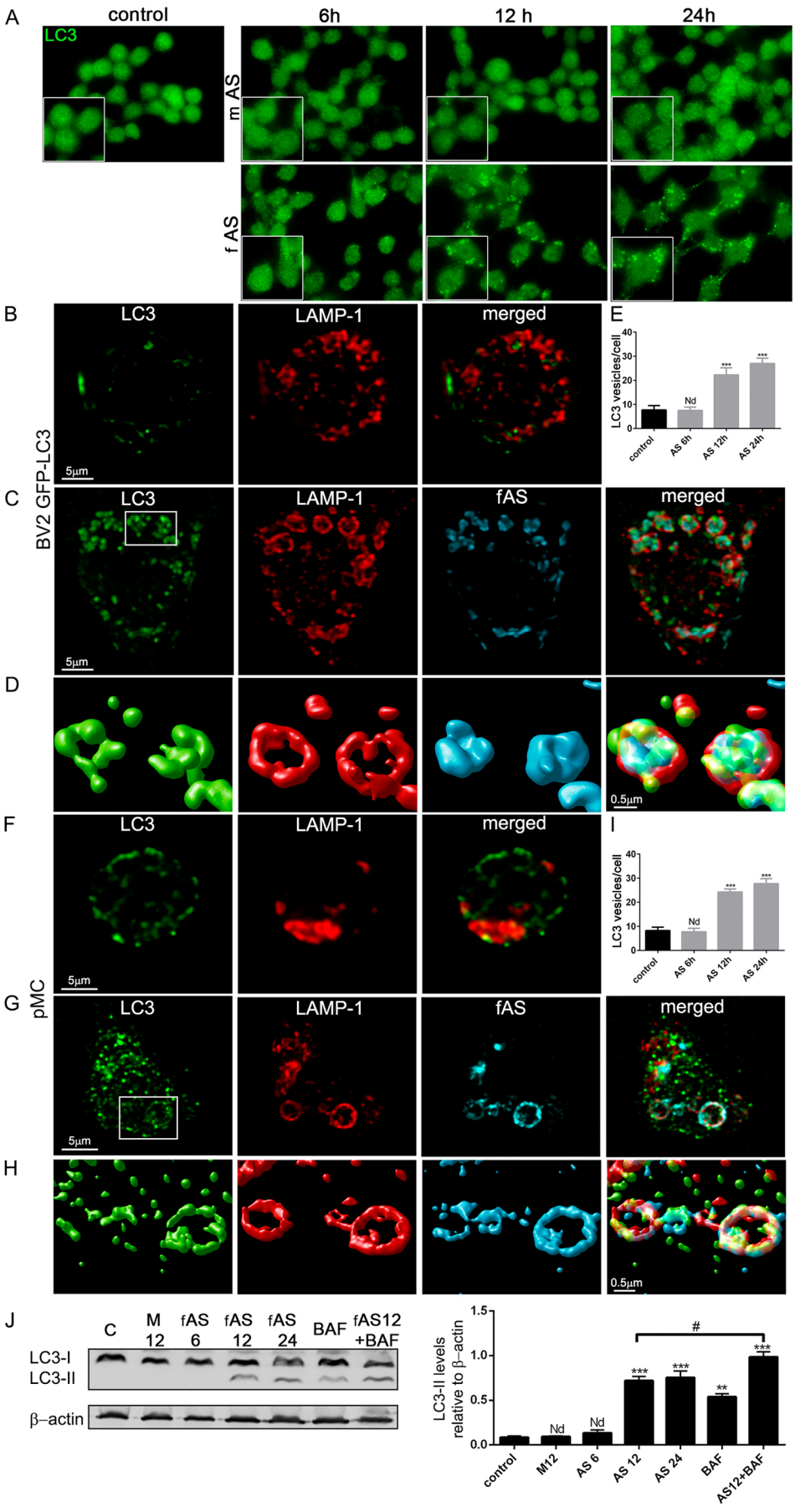

Fig. 1. Alpha-synuclein induces autophagy in microglial cells. (A) BV2 microglial cells were left untreated or stimulated at different time points with AS monomers (mAS) or fibrils (fAS) at 1 µM. Cells were then fixed and stained for LC3. (B–H) BV2 GFP–LC3 cells (B,C) or primary microglial cells (F,G) were left untreated or stimulated with Alexa Fluor 647-labelled AS fibrils (1 µM). After 12 h cells were immunostained with anti-LAMP1 (red) antibody and primary microglial cells were also stained for LC3. Images shown are *z*-stack projections. (D,H) 3D surface-rendered magnifications of the selected area above. (E,I) Mean±s.e.m. LC3-positive vesicles in unstimulated or treated BV2 (E) and primary microglial cells (I) were determined using ImageJ particle counting plugin after cell deconvolution (n=20). (J) Cell lysates from BV2 cells cultured with AS fibrils or monomers (1 µM) were collected at different time points and LC3 and β-actin protein levels were examined using western immunoblotting. Bafilomycin A1 (BAF) was added for the last 3 h. Graph shows quantification of mean±s.e.m. LC3-II expression relative to β-actin using densitometry. Results from at least three independent experiments were analysed by one-way ANOVA followed by post-hoc Dunnet's test; n=3. $^{**}P$<0.01; $^{***}P$<0.001; $^{\#}P$<0.01 when comparing AS at 12 h (AS12) with AS at 12 h in the presence of BAF (AS12 +BAF); Nd, no significant difference. pMC, primary microglial cells.

and it induces autophagy in microglial cells. The monomeric conformation was not able to activate the autophagy pathway at the time and dose studied.

Autophagy dynamics of AS-stimulated microglial cells

To further study the autophagic response triggered by fAS in microglial cells, we conducted live-imaging experiments at different time points after fAS stimulation. We used BV2 GFP–LC3 microglial cells and LysoTracker Blue for lysosomal staining. We did not observe a significant increase in LC3 puncta during the first 8 h after fAS stimulation (Fig. S1B–D, Fig. S2A–C; Movies 1–4). Of note, fAS was quickly internalised during the first 20 min by microglial cells and showed lysosomal localisation from the earliest time points (Fig. S1B–D; Movie 5).

Interestingly, after 12 h of stimulation we detected a substantial increase in the autophagy response. LC3 vesicles increased over time and were predominantly associated with LysoTracker+/fAS+ vesicles, forming a ring-like structure around them, as observed previously using confocal analysis (Fig. 2A,B; Fig. S2C; Movies 6, 7). In additional experiments, BV2 cells stably expressing GFP–ATG13 were co-transfected with a CFP–LC3 plasmid. ATG13 integrates the autophagy initiation complex ULK1, the most upstream complex of the autophagy pathway and is essential for autophagosome formation (Axe et al., 2008; Karanasios and Ktistakis, 2015). In agreement with previous reports and autophagy dynamics studies (Ktistakis et al., 2014), we observed positive ATG13 signal as an early event during autophagosome formation, closely associated with LC3 puncta, and its lifetime was shorter than the same structures containing LC3 (Fig. 2C,D; Fig. S2C; Movies 8, 9). As seen before, the LC3 signal associated with ATG13 progressed into characteristic rounded structures around synuclein fibrils (Fig. 2C,D).

Taken together, these results indicate that the autophagic response to fAS follows a canonical route (utilising ATG13-positive structures that mature into LC3-positive structures), but it is not an immediate event after synuclein treatment. The fact that lysosomes containing fAS are surrounded by LC3 vesicles suggests the possibility that the autophagic machinery may respond to lysosomal damage caused by the fibrils, and this is a question we will address later.

CLEM study of fAS-stimulated microglial cells reveals canonical autophagy

There are increasing numbers of reports showing the involvement of the non-canonical autophagy pathway in diverse pathological conditions since it was described for the first time. Although important advances have been made in the molecular characterisation and differentiation between these alternative routes, we are still far from precisely understanding the mechanistic details and limits of both pathways (Dupont et al., 2017; Martinez et al., 2015). The principal difference between autophagosomes and non-canonical vacuoles is that the former have two limiting membranes positive for LC3, whereas the latter have one. In order to discriminate these different processes, we conducted CLEM experiments and analysed the presence of single- or double-membrane LC3-positive vesicles after fAS stimulation of BV2 GFP–LC3 microglial cells.

We clearly detected double-membrane autophagic vesicles (AV) mainly correlating with GFP–LC3 signal and closely associated with fAS+ structures (Fig. 3A–F; Movies 10–12). Furthermore, we also observed double-membrane vesicles and multi-membrane structures surrounded by a single-limiting membrane, probably as a result of fusion events between autophagosomes and lysosomes (Fig. 3A–F; Movies 10–12). These results are in agreement with a previous report describing similar AVs found on neocortical biopsies of human brain from individuals with Alzheimer's disease (Nixon et al., 2005). In agreement with Nixon et al., the morphologies and composition of vesicles that accumulated after fAS treatment corresponded to those of the vesicular compartments of the autophagic pathway. Although we did not find sufficient evidence of quantitative ultrastructural analyses of glial organelles in the literature (Bisht et al., 2016), most of the vesicles we observed in fAS-stimulated microglial cells correlated with standard morphometric criteria for the immature and mature autophagosomes as expected for neural cells (Dunn, 1990a,b). These criteria include a size >0.5 µm in diameter, a double-limiting membrane (immature), and the presence within a single vesicle of multiple membranous domains from organelle sources such as the Golgi, mitochondria or endoplasmic reticulum (Fig. 3A–F; Movies 10–12). We also observed similar AV morphology in non-treated microglial cells, although single-membrane vesicles presented a smaller size in comparison to stimulated cells (Fig. S2D,E). Moreover, in order to improve the detection of autophagosomes around fAS+ vesicles, we carried out additional CLEM experiments with fAS-stimulated microglial cells previously treated with BAF. Similar to our previous results, we found examples where an autophagosome was in close proximity to a larger AV (Fig. 3I,J) and as expected, we also detected areas where double-membrane autophagosomes accumulated around other AVs (Fig. 3G,H; Movie 13).

To more precisely examine the ultrastructural nature of the AV formed after AS stimulation in microglial cells, we conducted live-cell CLEM assays. We stimulated BV2 GFP–LC3 cells with fAS for 12 h and we followed the autophagy response using time-lapse widefield imaging and subsequent EM analysis (Fig. 4A,B). As we observed previously, an LC3 ring-like structure was formed around fAS (Fig. 4A). Interestingly, we found that the LC3-positive area predominantly correlated with a central double-membrane autophagosome closely located to other single- and double-membrane vesicles that were also positive for fAS signal (Fig. 4D,E,F; Movies 14, 15). In an additional live-cell CLEM experiment (Fig. 4C,G,H,I; Movies 16, 17) we observed that the region positive for LC3 signal correlated with concentric multi-membrane structures with a central double-membrane vesicle exhibiting a dense core. Moreover, these structures were in close contiguity with ER membranes, suggesting that the ER could be a main membrane donor in this process. These observations are in concordance with a previous electron tomography study showing that the ER associates with early autophagic structures and acts as a membrane source for autophagosome formation (Hayashi-Nishino et al., 2009).

Overall, these results provide evidence of canonical autophagy, instead of LAP, as the main effector pathway in microglial cells after fAS internalisation.

Effects of fAS on lysosomal and mitochondrial quality of microglial cells

Galectin-3 (GAL-3, also known as LGALS3) is a sugar-binding protein that recognises beta-galactoside and is usually only present on the exterior leaflet of the plasma membrane and the interior leaflet of intracellular vesicles (Sundblad et al., 2011). GAL-3 relocalisation has previously been utilised to identify ruptured vesicles when bacteria and viruses enter the cytoplasm during infection (Maier et al., 2012; Thurston et al., 2012). Recent studies

Journal of Cell Science (2018) 131, jcs226241. doi:10.1242/jcs.226241

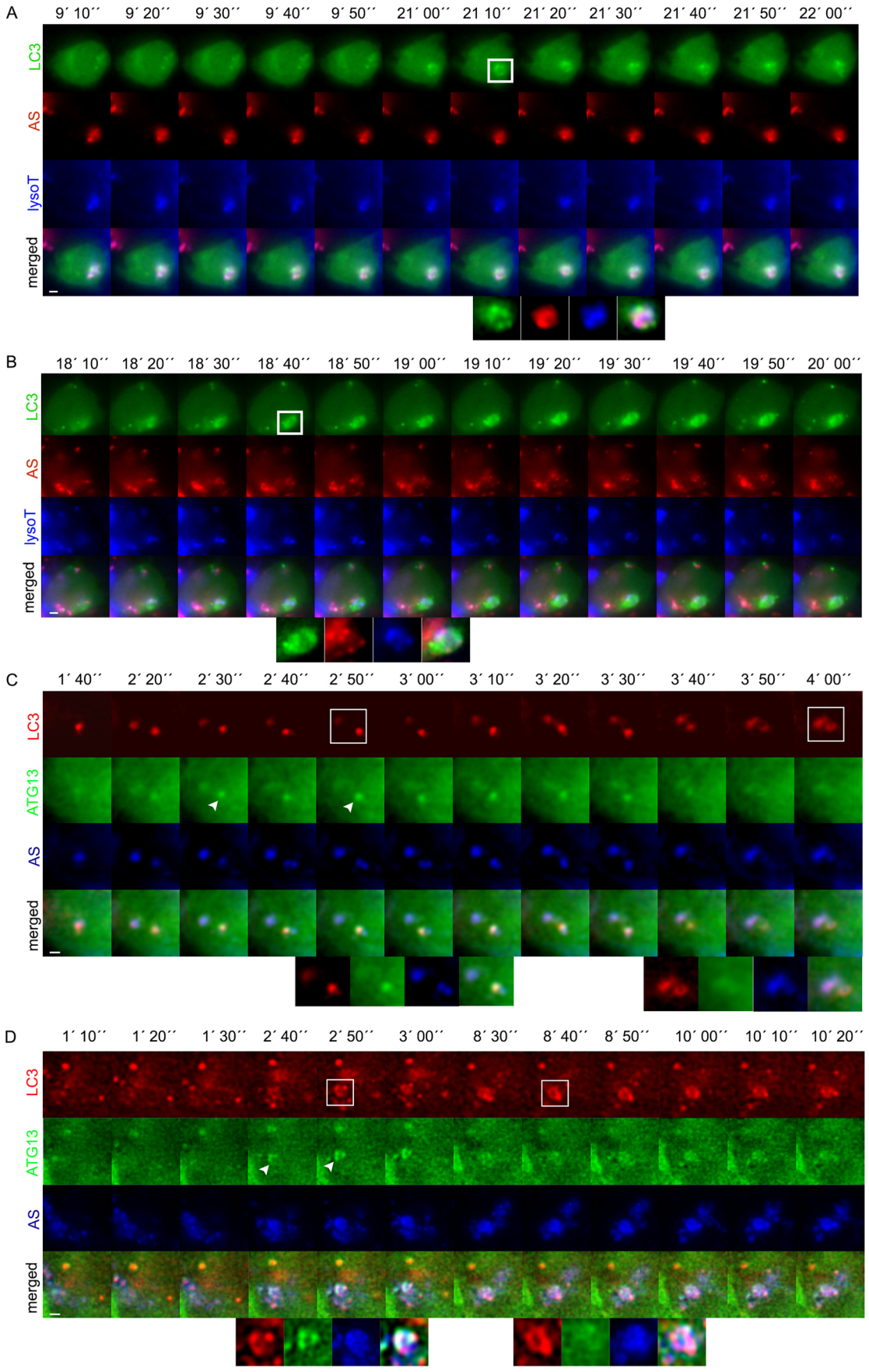

Fig. 2. See next page for legend.

Journal of Cell Science (2018) 131, jcs226241. doi:10.1242/jcs.226241

Fig. 2. Evaluation of LC3 and ATG13 dynamics in AS-stimulated microglial cells using **live-imaging.** (A,B) BV2 cells stably expressing GFP–LC3 (green) were stimulated with fAS (red) for 12 h. Imaging was performed at 1 frame per 10 s for 1 h and a selected interval within this sequence for two experiments is shown. LysoTracker Blue was added 30 min previous to image acquisition. Note that autophagosomes form a ring-like structure around LysoTracker+/fAS+ structures. (C,D) BV2 cells stably expressing GFP–ATG13 (green) were transfected with CFP–LC3 (red) and stimulated with fAS (blue) and imaged as described above. Arrowhead indicates the first discernible ATG13 punctum during autophagosome formation (C) and ATG13 forming a puncta pattern similar to LC3 (D). Scale bars: 2 µm.

have also demonstrated that even in the absence of bacteria or viruses, some galectins can translocate to damaged lysosomes before their removal by the autophagic pathway (Freeman et al., 2013). Since lysosomal damage is one of the possible mechanisms inducing autophagy in the cells in our experiments, we used a recently described protocol to assess lysosomal damage recognised by GAL-3 (Aits et al., 2015). We stimulated BV2 and primary microglial cells with labelled fAS at different time points and used confocal microscopy to assess whether GAL-3 translocated to damaged lysosomes (Fig. 5). L-leucyl-L-leucine methyl ester (LLOMe), which induces lysosome-specific membrane damage (Uchimoto et al., 1999), was used as a positive control (Fig. 5A,B). In accordance with the autophagy dynamics previously described, we detected a substantial change, from diffuse to punctate staining pattern, after 12 h of fAS treatment but not during earlier time points or after monomeric AS stimulation (Fig. 5C,F,G). In addition, we observed a high extent of co-localisation of GAL-3 with both fAS and LAMP-1 (Fig. 5C,D).

We next evaluated whether the LC3-positive vesicles formed after fAS stimulation co-localised with GAL-3 puncta and found a high degree of co-localisation (Fig. 5E). This suggests that lysosomal damage acts as a positive signal for autophagy activation in fAS-stimulated microglial cells. These results are in agreement with Flavin et al. (2017), who described that lysosomes ruptured by AS in SH-SY5Y neuronal cells are targeted for autophagic degradation. We also assessed whether fAS could disturb lysosomal activity, using a cathepsin-B fluorometric assay to monitor enzyme activity at different time points after microglial cell stimulation. We found a significant increase in cathepsin-B activity after 8 h of treatment, which diminished to basal levels after 12 h (Fig. 5H), coincident with lysosomal impairment detection.

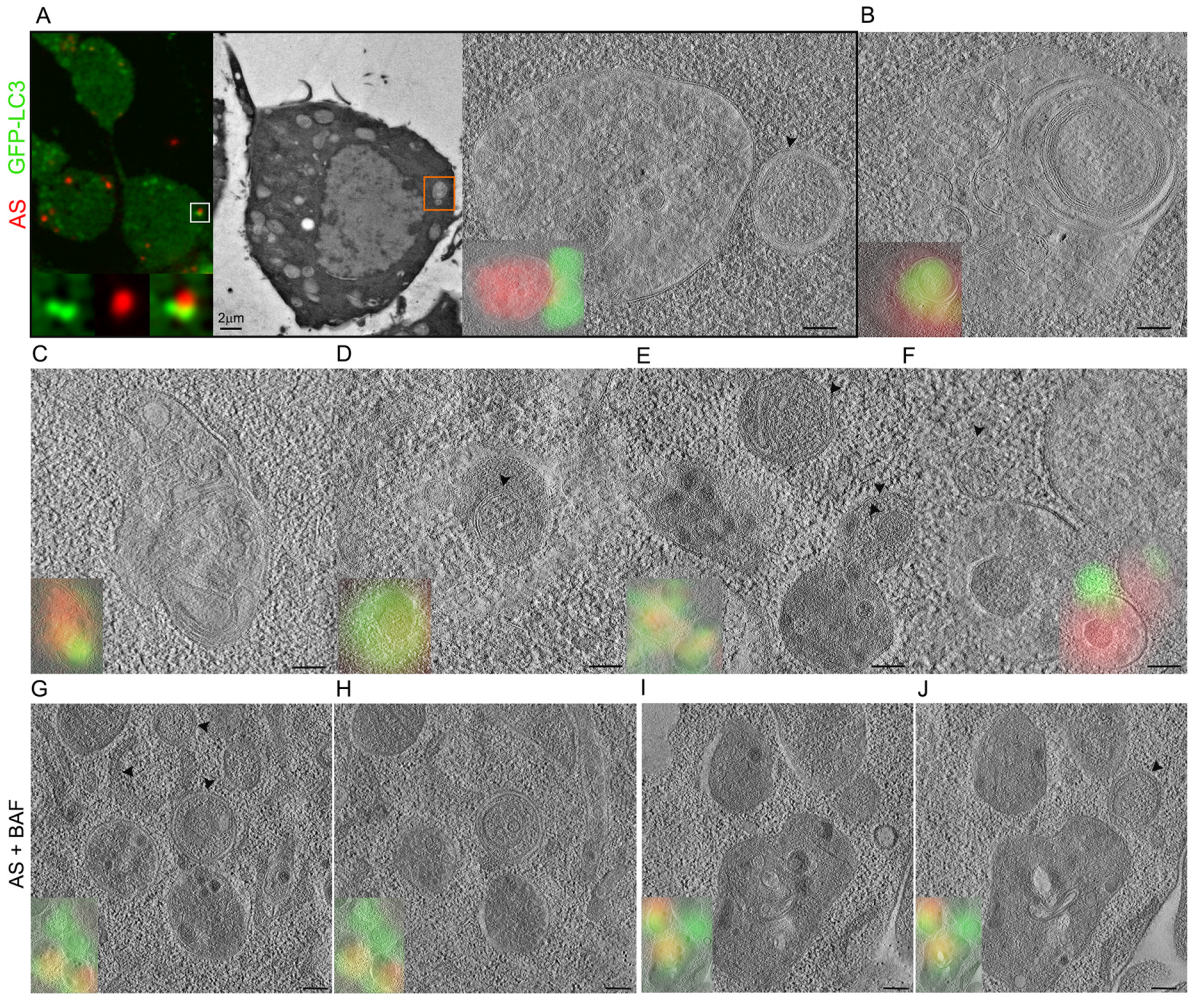

Fig. 3. Correlative light-electron microscopy study of LC3-positive vesicles in fAS-stimulated microglial cells. BV2 GFP–LC3 (green) cells were stimulated with fAS (red) for 12 h and incubated in the absence (A–F) or the presence (G–J) of BAF for the last 3 h. Cells were then fixed using high-pressure freezing (HPF) and processed for optical and electron microscopy (EM) acquisition. 300 nm sections were imaged using fluorescence microscopy and EM tomograms were acquired at the regions of interest. (A) Wide-field and low- (200×) and high-magnification (20,000×) electron microscopy images with the overlay result. (B–J) High-magnification slides (20,000×) from tomograms of a selection of representative experiments indicating the CLEM result. Scale bars: 200 nm. Arrowheads indicate double-membrane vesicles.

Journal of Cell Science (2018) 131, jcs226241. doi:10.1242/jcs.226241

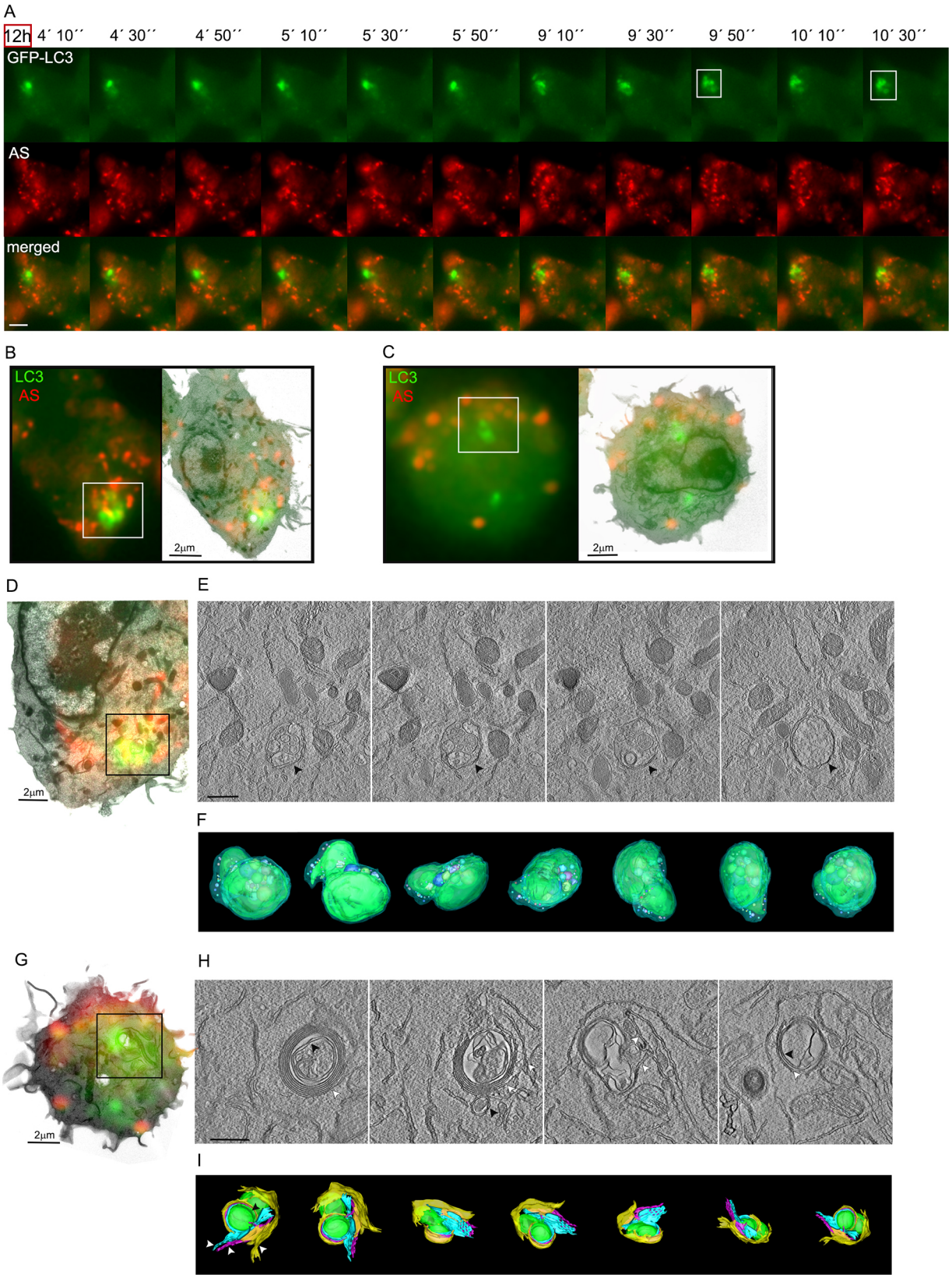

Fig. 4. See next page for legend.

These results indicate that lysosomes respond to the presence of fAS increasing cathepsin-B activity, which decreases with the progression of lysosomal damage.

In parallel experiments, we also evaluated mitochondrial status, as mitochondrial dysfunction has been associated with several neurodegenerative diseases and AS has been shown to alter

Fig. 4. Live-cell CLEM imaging of fAS-stimulated microglial cells. (A) BV2 GFP–LC3 cells (green) were stimulated with fAS (red) for 12 h. Imaging was performed at 1 frame per 20 s. After detecting the event of interest (white box), cells were immediately fixed and processed for EM tomography. Twenty serial tomograms were acquired on 300 nm sections. Scale bar: 5 µm. (B,D) Correlation result from the cell shown in A, indicating the area acquired at high magnification (9400×) in each tomogram. (E) Representative slides of the serial tomogram following identification of the event of interest in panel D are shown. Scale bar: 500 nm. Arrowhead indicates a central double-membrane autophagosome. (C,G) Correlation result of a second live-cell CLEM experiment indicating the area acquired at high-magnification (9400×) in each serial tomogram. BV2 GFP–LC3 cells were stimulated and imaged as described in A. (H) Representative slides of the serial tomogram following identification of the event of interest in panel G are shown. Scale bar: 500 nm. Arrowheads indicate a double-membrane autophagosome surrounded by ER membranes (white arrows). (F,I) 3D reconstructions of the vesicles shown in the serial tomogram slides in panels E and H, respectively.

mitochondrial activity (Esteves et al., 2011). However, we did not find changes either in mitochondrial mass nor mitochondrial cell membrane potential after fAS stimulation at the time points studied (Fig. 5I). Overall these findings indicate that fAS induces lysosomal but not mitochondrial damage, with a similar kinetic to that observed in autophagy activation, suggesting that this response is concomitant to lysosomal impairment.

TBK1 and OPTN are recruited to damaged lysosomes in AS-stimulated microglial cells

Previous studies performed in *Salmonella enterica*-infected HeLa cells have shown that TBK1 directly phosphorylates the autophagic adaptor OPTN and that this interaction allows the autophagic machinery to be recruited to the intracellular loci of the bacteria, resulting in elimination of the bacteria by lysosomes. Furthermore, OPTN has been observed in protein inclusions of various neurodegenerative diseases, such as ALS and PD. Thus, we aimed to determine whether TBK1 and OPTN could be recruited to damaged lysosomes in AS-stimulated microglial cells.

As the autophagy response was triggered at a similar time point to that described for AS-induced lysosomal damage (Fig. 5C–G, 12 h time point), we aimed to determine whether microglial autophagy could be activated as a means to control lysosomal quality rather than by AS internalisation itself. Therefore, we analysed the dynamics of TBK1 and OPTN activation in AS-stimulated microglial cells using immunoblot and confocal immunofluorescence.

Interestingly, we found that levels of TBK1 and OPTN phosphorylation were significantly increased after 12 h of fAS stimulation but not during earlier time points or after AS monomeric stimulation (Fig. 6A,B).

In parallel experiments, we observed using confocal microscopy that TBK1 and OPTN co-localise with ubiquitin and Gal-3 puncta in AS-stimulated BV2 and primary microglial cells (Fig. 6C; Fig. S3), indicating the recruitment of both proteins to ubiquitylated lysosomal damage sites. In accordance with our previous results (Fig. 6A, Fig. 5), TBK1 and OPTN puncta formation were only observed after 12 h of fAS stimulation, which contrasted with the diffuse staining pattern observed in the control conditions (Fig. S3A,B). Moreover, we also observed LC3- and AS-positive vesicles co-localizing with both TBK1 and OPTN (Fig. 6D).

In additional experiments, we used confocal immunofluorescence to analyse whether the autophagy receptors p62 and NDP52 would also be recruited to fAS-positive vesicles. Although mouse NDP52 is a truncated form lacking the C-terminal zinc-finger domain that interacts with ubiquitin, it has been shown to bind phosphorylated TAU via the SKICH domain and to facilitate autophagy-mediated degradation of TAU in mouse (Jo et al., 2014; Minowa-Nozawa et al., 2017), indicating that NDP52 recognises different targets through different domains. Nonetheless, we did not observe co-localisation of either NDP52 or p62 with fAS after 12 h of stimulation (Fig. S4A,F). As expected, NDP52 did not co-localise with ubiquitin in fAS-stimulated microglial cells (Fig. S4C). Moreover, we did not find an increase in p62 puncta formation after fAS stimulation in microglial cells (Fig. S4D,E), suggesting these adaptors do not function together in targeting fAS-containing organelles.

Taken together, these results show that TBK1 and OPTN activation and recruitment to damaged lysosomes displays a similar kinetic to that described for autophagy induction (Figs 1, 2), suggesting both proteins participate in the autophagic turnover of this organelle and that microglial autophagy is activated as a response to AS-induced lysosomal impairment.

TBK1 inhibition impairs LC3 recruitment to damaged lysosomes

In a previous report, Moore and Holzbaur (2016) showed that TBK1 and OPTN are recruited to mitochondria after acute damage, and that loss or chemical inhibition of TBK1 disrupts mitophagy. We next aimed to determine whether TBK1 inhibition would affect autophagy adaptor recruitment and LC3 targeting of damaged lysosomes in fAS-stimulated microglial cells. Firstly, we evaluated the effectiveness of BX795, MRT67307 and Amlexanox, three chemical inhibitors of TBK1. As shown in Fig. 7A, all three treatments supressed TBK1 phosphorylation in fAS-stimulated microglial cells.

Next, we analysed LC3 puncta formation and LC3-II induction in fAS-stimulated BV2 GFP–LC3 microglial cells pre-treated with Amlexanox, which has been reported as one of the most specific inhibitors of TBK1 (Reilly et al., 2013; Yu et al., 2015). We observed a marked decrease of both LC3-positive vesicles and relative LC3-II protein levels in cells with impaired TBK1 activity (Fig. 7B,C,E). Moreover, treatment with Amlexanox correlated with a decrease in p-TBK1 and OPTN puncta formation after fAS stimulation in microglial cells (Fig. 7F–I). As expected, GAL-3 puncta formation was not affected by TBK1 inhibition in fAS-stimulated microglial cells (Fig. 7J), suggesting that lysosomal damage is a result of fAS accumulation and occurs independently of TBK1 activity.

Additionally, inhibition of TBK1 did not modify LC3 puncta levels in microglial cells treated with the mTORC1 inhibitor PP242 (Fig. 7D,E), which indicates that only autophagy activated by lysosomal damage was affected by TBK1 inhibition.

Overall, our results showed that OPTN and LC3 recruitment to damaged lysosomes in fAS-stimulated microglial cells was dependent on TBK1 activity.

Autophagy prevents cell death in fAS-stimulated microglial cells

Autophagy is intimately associated with eukaryotic cell death and apoptosis. However, the molecular connections between autophagy and cell death are complex and, in different contexts, autophagy may promote or inhibit cell death (Arroyo et al., 2013; Degenhardt et al., 2006; Green and Levine, 2014). We therefore evaluated the effect of autophagy inhibition on microglial cell survival. We inhibited autophagy through the use of using spautin-1, which promotes the degradation of VPS34 PI3 kinase complexes by inhibiting two ubiquitin-specific peptidases, USP10 and USP13 that target the Beclin1 subunit of VPS34 complexes (Liu et al., 2011). In addition, we also used a siRNA targeting FIP200, a pivotal

Journal of Cell Science (2018) 131, jcs226241. doi:10.1242/jcs.226241

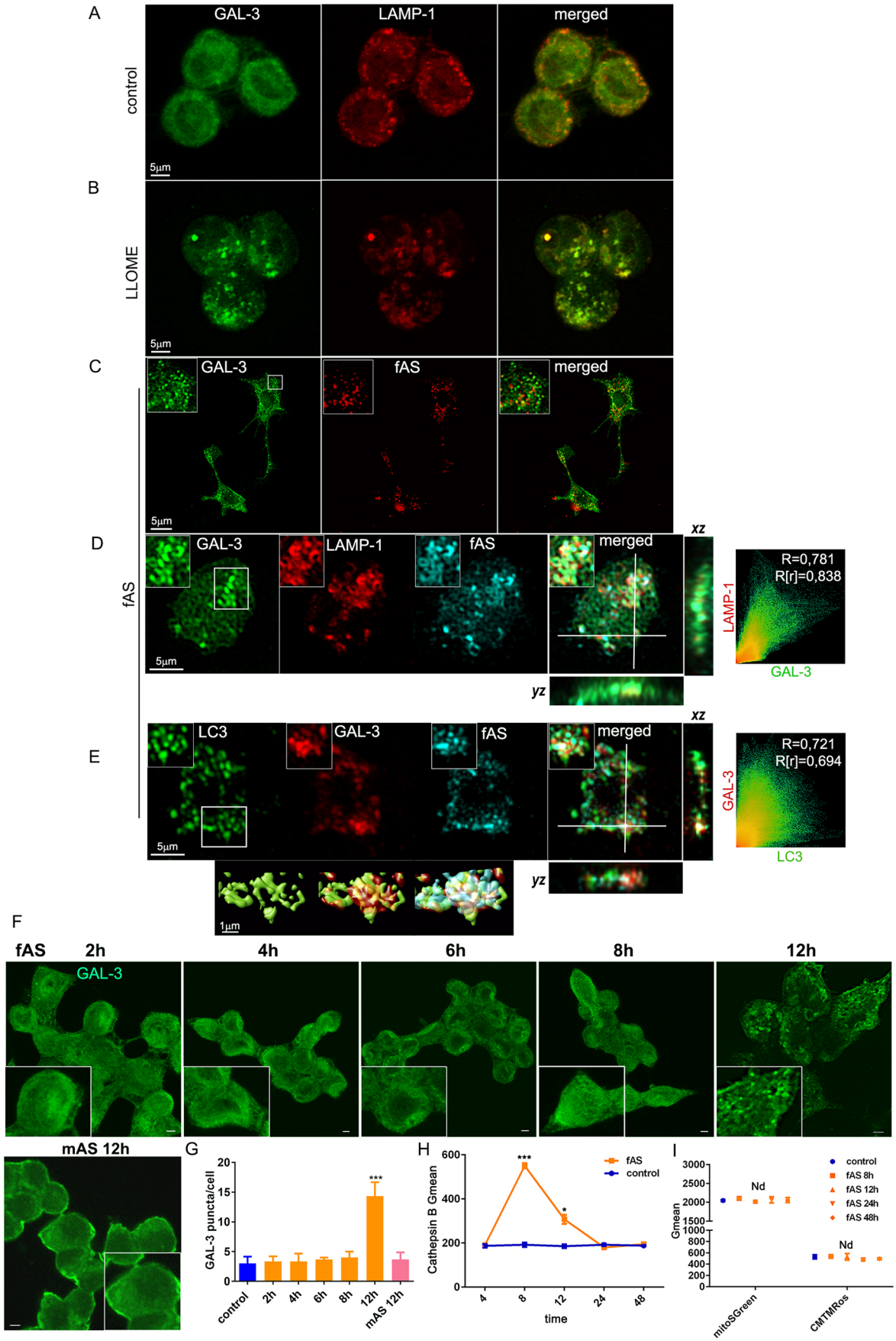

Fig. 5. See next page for legend.

Fig. 5. Evaluation of lysosomal damage in fAS-stimulated microglial cells. (A,B) BV2 cells were left untreated (A) or stimulated (B) with LLOME (500 µM) for 2 h. Next, cells were immunostained with anti-GAL-3 (green) and anti-LAMP-1 (red) antibodies. (C–E) BV2 (C) or primary (D,E) microglial cells were treated with fAS for 12 h. Cells were then fixed and stained for GAL-3 and LAMP-1 or LC3, as indicated. Merged images show orthogonal views and co-localisation analysis between the specified labels. Pearson coefficient (R) and overlap coefficient (R[r]) are listed. (F) BV2 microglial cells were stimulated with fibrillary (fAS) or monomeric (mAS) AS at the indicated time points. Scale bars: 5 µm. (G) Next, cells were immunostained for GAL-3 and puncta formation was determined using ImageJ particle counting plugin. (H,I) BV2 cells were stimulated with fAS (5 µM) at different time points or left untreated. Microglial cells were then stained with Magic Red dye for evaluation of cathepsin-B activity (H), MitoSpy Green FM for measuring mitochondrial mass or MitoSpy Orange CMTMRos for assessing mitochondrial membrane potential changes (I). Graphs show quantification of mean fluorescence intensity (Gmean) using flow cytometry. Results were analysed by one-way ANOVA followed by post-hoc Dunnet's test; n=3. Error bars represent s.e.m. (*P<0.05; ***P<0.001).

protein required for autophagy induction and autophagosome formation (Hara et al., 2008). We evaluated the ability of spautin-1 and FIP200 siRNA to inhibit autophagy, using confocal microscopy analysis of LC3 puncta formation after treating BV2 GFP–LC3 microglial cells with PP242, a specific mTORC1 inhibitor and autophagy inducer. We observed that both treatments significantly suppressed the autophagy response (Fig. S5A,B). Moreover, autophagy blockade by spautin-1 and FIP200 siRNA also decreased LC3 puncta formation in fAS-stimulated primary microglial cells (Fig. S5C).

We next investigated whether autophagy inhibition prior to fAS stimulation affects microglial cell viability. BV2 and primary microglial cells were cultured in the presence or the absence of spautin-1 or FIP200 siRNA and stimulated with fAS for 24 h, then we evaluated microglial cell death using flow cytometry. We found an increase in the frequency of dead cells (positive for both propidium iodide and Annexin V) when autophagy was inhibited by spautin-1 or FIP200 siRNA in fAS-stimulated microglial cells. Similar results were obtained with both BV2 and primary microglial cells (Fig. 8A,B).

Mitochondrial outer membrane permeabilisation (MOMP) is often required for activation of the caspase proteases that cause apoptotic cell death. As a consequence, mitochondrial outer membrane integrity is highly controlled, primarily through interactions between pro- and anti-apoptotic members of the B-cell lymphoma 2 (BCL-2) protein family (Tait and Green, 2010). BCL-2 and BCL-xL (also known as BCL2L1) anti-apoptotic proteins promote cell survival by preventing mitochondrial membrane permeabilisation and subsequent content release that leads to caspase activation and ultimately, programmed cell death (Shamas-Din et al., 2013). Lysosomal damage and resulting lysosomal membrane permeabilisation have been shown to induce apoptosis through MOMP, which can be brought about by cathepsin-mediated activating cleavage of pro-apoptotic BID or inhibiting cleavage of anti-apoptotic BCL-2 and BCL-xL proteins (Aits and Jaattela, 2013; Cirman et al., 2004; Droga-Mazovec et al., 2008). Here, we also used flow cytometry to evaluate the expression levels of BCL-2, BCL-xL and cleaved caspase-3 in fAS-stimulated BV2 microglial cells in the presence or the absence of both autophagy inhibitors, spautin-1 and FIP200 siRNA. We found a decrease in BCL-2 and BCL-xL protein levels with a concomitant increase in cleaved-caspase-3 expression when autophagy was impaired (Fig. 8C). In parallel experiments we analysed mitochondrial mass and membrane potential changes after autophagy inhibition in fAS-stimulated microglial cells. We detected an increase in mitochondrial mass, but a decrease in mitochondrial membrane potential, after inhibition of autophagy (Fig. 8D,E). Moreover, autophagy inhibition also led to the accumulation of damaged lysosomes in fAS-stimulated microglial cells. This was evidenced by an increase in GAL-3 puncta at earlier time points after treatment and diminished LysoTracker Red DND-99 staining (Fig. 8F–H). Taken together, these results indicate the autophagy requirement for mitochondrial and lysosomal homeostasis.

Collectively, our results showed that AS induced lysosomal damage and autophagy activation, and that the inhibition of this degradative pathway led to mitochondrial and lysosomal quality impairment, which includes MOMP, and consequent microglial cell death.

DISCUSSION

Misfolding and intracellular aggregation of AS are thought to be crucial factors in the pathogenesis of Lewy body diseases (LBDs), such as PD. Recent studies suggest that small amounts of AS are released from neuronal cells by unconventional exocytosis, and that this extracellular AS contributes to the major pathological features of LBD such as neurodegeneration, progressive spreading of AS pathology and neuroinflammation (Lee et al., 2014). In these neurodegenerative processes, the activation of microglia, which disturbs the homeostasis of the neuronal environment, is a common pathological finding. The behaviour of microglia is therefore a determinant of disease progression.

In our present study, we show using confocal microscopy and immunoblotting analysis that fAS, but not its monomeric conformation, induces autophagy in microglial cells. Our results are in accordance with previous observations showing that AS fibrils are more potent cellular activators than other aggregation states. In agreement with a recent article from our group, Hoffmann et al. found that fAS increased the production and secretion of pro-inflammatory cytokines in microglial cells to a greater extent than oligomers or monomers (Bussi et al., 2017; Hoffmann et al., 2016).

Autophagy is a highly dynamic pathway and live-cell imaging has been extensively used to follow autophagy events in real time (Karanasios and Ktistakis, 2015). Nonetheless, most previous studies monitoring the autophagic flux in glial cells were done using fluorescence microscopy of fixed cells and little is known about autophagy dynamics in microglial cells.

Here, we extensively characterised the autophagy dynamics of microglial cells stimulated with fAS using live-cell imaging. We observed that although fAS is quickly internalised by microglial cells, autophagy induction was evident after 12 h of stimulation (Figs 1, 2). Interestingly, we observed that LC3 decorated lysosomes containing fAS, forming a ring-like structure around them. In additional experiments with BV2 cells stably expressing ATG13, we detected ATG13-positive structures that progresses into LC3-positive vesicles, which coincides with previous autophagy dynamics reports (Karanasios and Ktistakis, 2015; Ktistakis et al., 2014) and suggests that the autophagic response to fAS follows a canonical pathway (Fig. 2C,D).

The kinetics of autophagy we observed contrasts with dynamics studies of LAP where phagosomes are rapidly decorated with LC3, usually within minutes (Martinez et al., 2011). Although we cannot rule out the involvement of the non-canonical pathway during this process, we could effectively corroborate by using high-precision and live-cell CLEM approaches that LC3-positive structures with double-membrane bound AV formed after fAS stimulation (Figs 3, 4), indicating a predominant role for the canonical autophagy pathway rather than its alternative route during this process.

Journal of Cell Science (2018) 131, jcs226241. doi:10.1242/jcs.226241

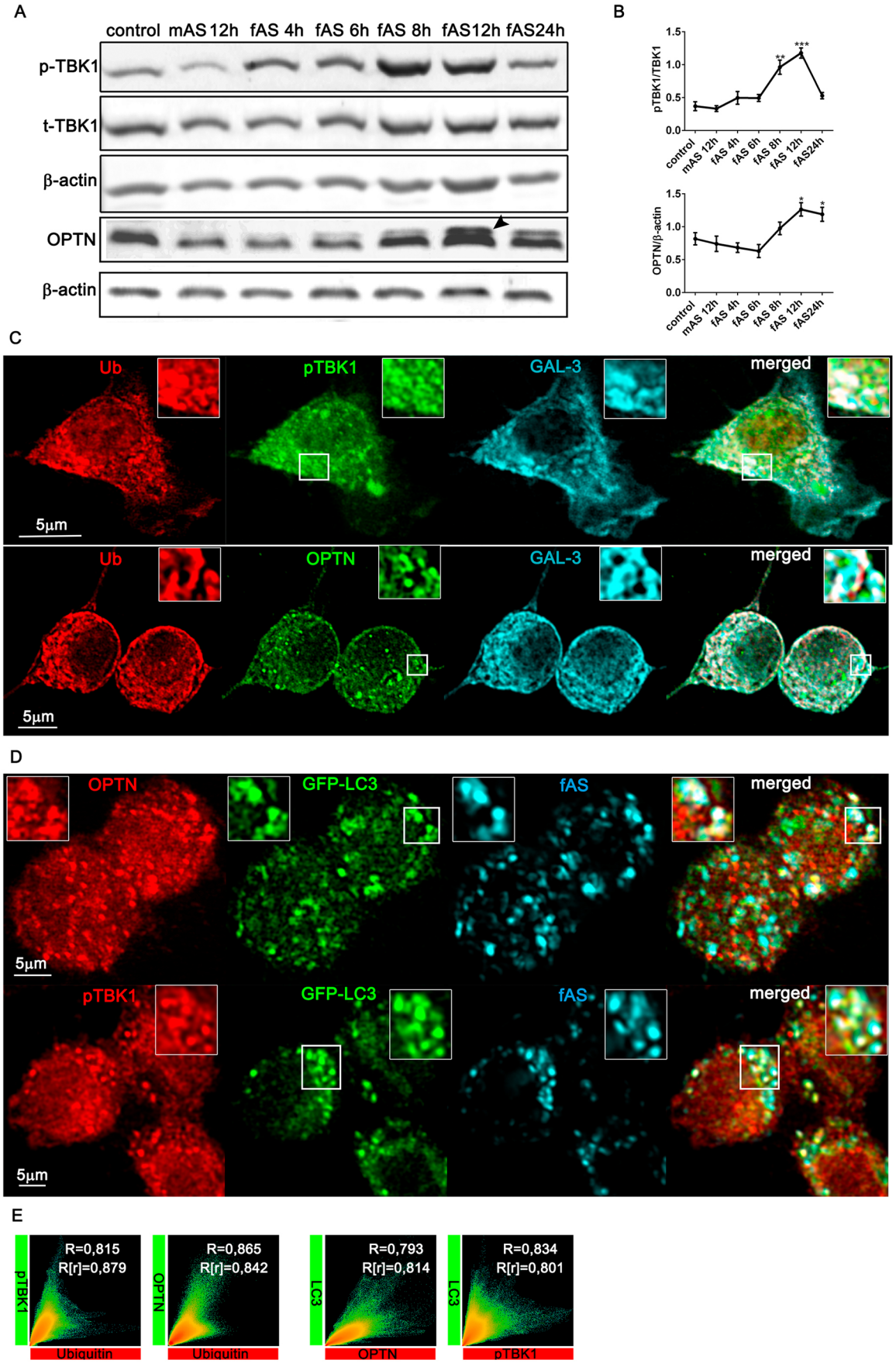

Fig. 6. See next page for legend.

Journal of Cell Science (2018) 131, jcs226241. doi:10.1242/jcs.226241

Fig. 6. TBK1 and OPTN are recruited after fAS stimulation in microglial cells. (A) BV2 cells were stimulated with fibrillar (fAS) or monomeric (mAS) AS at different time points and cell lysates were collected for western blot analysis. Arrowhead indicates shifted (phosphorylated) OPTN band. (B) Mean±s.e.m. band quantification of phosphorylated (p)TBK1 relative to total TBK1 (upper graph) and OPTN relative to β-actin levels (lower graph). Results from at least three independent experiments were analysed by one-way ANOVA followed by post-hoc Dunnet's test; n=3. *P<0.05; **P<0.01; ***P<0.001. (C) Primary microglial cells treated with fAS for 12 h were fixed and stained for ubiquitin (red), pTBK1 or OPTN (green) and GAL-3 (cyan). (D) BV2 GFP–LC3 cells (green) treated with fAS (cyan) for 12 h were fixed and stained for pTBK1 or OPTN (red). Image crops shows magnification of the selected areas (white box). (E) Co-localisation analysis between the specified labels in panels C and D. Pearson coefficient (R) and overlap coefficient (R[r]) are listed.

Recent evidence indicates that AS could disturb neuronal metabolism through inducing lysosomal and mitochondrial damage (Bourdenx et al., 2014; Freeman et al., 2013; Xilouri et al., 2016). Nevertheless, the effects of AS on glial organelles is poorly understood. Here, we report that although fAS is rapidly incorporated into lysosomes after cellular internalisation, it induces lysosomal damage and TBK1/OPTN recruitment at the same time point as when the autophagy response is substantially activated (Figs 5, 6; Fig. S3). Moreover, we discovered a high degree of co-localisation between LC3 and GAL-3 puncta, and between LC3 and TBK1 and OPTN puncta, suggesting that lysosomal damage rather than fAS acts as an activator signal for autophagy induction. Importantly, we observed that TBK1 inhibition disrupts OPTN and LC3 recruitment to damaged lysosomes in fAS-stimulated microglial cells, but it did not affect autophagy induced by inhibition of mTORC1. Collectively, these results suggest that OPTN is recruited to lysosomes damaged by persistent fAS accumulation, following recognition of OPTN by TBK1 and phosphorylation of TBK1, which may allow subsequent recruitment of LC3 and the autophagy machinery as a cellular attempt at restoring lysosomal quality control.

Along this line of evidence, Flavin et al. (2017) observed, using immunofluorescence microscopic analysis of sections from PD patients, that Lewy bodies (LBs) and other amyloid aggregates were surrounded by GAL-3, suggesting that endocytic vesicle rupture is a conserved damaging mechanism of cellular invasion by amyloid proteins.

In agreement with our results, Freeman et al. (2013) showed that AS induces lysosomal rupture and cathepsin-B release in neuronal cells after endocytosis. In addition, cysteine cathepsins were shown to be pivotal for lysosomal degradation of AS fibrils (McGlinchey and Lee, 2015). Although we observed a sharp increase in cathepsin-B levels 8 h after fAS stimulation, it notably diminished 12 h after treatment, which could indicate an overwhelmed lysosomal ability to degrade AS aggregates, leading ultimately to lysosomal damage (Fig. 7A). Collectively, considering the evidence and data shown here, we propose that accumulation of pathological protein aggregates and the formation of inclusions such as LBs arise from the failure of cellular attempts to degrade ruptured vesicles (and their amyloid contents) through the autophagy–lysosome pathway.

Although previous reports have indicated that AS induces mitochondrial damage in neurons (Bir et al., 2014; Martin et al., 2006), we did not find significant changes either in mitochondrial mass or membrane potential at the time points studied, indicating that fAS does not alter mitochondrial quality during the first 48 h of stimulation in microglial cells (Fig. 7B).

There are increasing numbers of research articles providing evidence about the pivotal role of autophagy during CNS homeostasis and disease progression (Hara et al., 2006; Komatsu et al., 2006; Nikoletopoulou et al., 2015). However, the role of autophagy in glia and the contribution of defective glial autophagy in neurodegeneration remain poorly characterised.

In this report, we analysed the effect of disrupting autophagy on microglial cell survival after fAS stimulation. We observed increased levels of cell death of fAS-stimulated microglial cells after both spautin-1 treatment and downregulation of FIP200 with siRNA (Fig. 7C,D). Our findings agreed with a previous report indicating that neural-specific deletion of FIP200, involved in autophagosome biogenesis, caused axonal degeneration in cerebellar neurons, eventually leading to their death (Liang et al., 2010).

The mitochondria-mediated caspase activation pathway is a major apoptotic pathway characterised by MOMP and subsequent release of cytochrome C into the cytoplasm to activate caspases. MOMP is regulated by the BCL-2 family of proteins, which act as inducers or blockers of the process (Xiong et al., 2014). Of relevance to this work, it has been shown that lysosomal damage can induce MOMP-dependent cell death, and lysosomal proteases released into the cytosol have been implicated in apoptotic cell death (Repnik et al., 2014). In the present study, we found that autophagy inhibition increased mitochondrial mass but impaired mitochondrial membrane potential, downregulated BCL-2 and BCL-xL protein levels and increased cleaved caspase-3 protein expression in fAS-stimulated BV2 cells, which suggests activation of apoptosis (Fig. 7E,F). Moreover, autophagy blockade led to the accumulation of ruptured lysosomes after fAS stimulation in microglial cells, which indicates a requirement for functional autophagic activity in the removal of damaged lysosomes. Although lysosomal damage may have an autophagy-blocking effect under persistent stress conditions, experimental evidence, in agreement with our results, has shown that lysosomes damaged by lysosomotropic reagents are selectively isolated by autophagy and disruption of this pathway caused inhibition of lysosomal biogenesis (Maejima et al., 2013).

Although we cannot disregard additional upstream signals triggering MOMP, we consider it likely that lysosomal damage, together with the inability of the autophagic pathway to clear this organelle, leads to MOMP and ultimately to cell death. Collectively, our results suggest a protective role for the autophagy pathway in fAS-stimulated microglial cells.

Extracellular AS has emerged as a crucial player in the pathogenesis of LBDs and other synucleinopathies such as PD and multiple system atrophy (Lee et al., 2014). Recent studies have provided evidence that extracellular AS alone, particularly in fibrillar form, can be responsible for all the major pathological changes in neurodegenerative diseases: aggregate deposition and spreading, neuroinflammation and neurodegeneration (Peelaerts et al., 2015). Although several articles have indicated that extracellular AS activates microglial cells (Bussi et al., 2017; Codolo et al., 2013; Hoffmann et al., 2016), this is, to the best of our knowledge, the first study showing that fAS recruits TBK1 and OPTN to ubiquitylated lysosomes and induces autophagy in microglial cells. In addition, we also characterised the microglial autophagy dynamics by correlating light-microscopy imaging with the specific ultrastructural morphology of the autophagic compartments participating during this process.

These findings provide new insights into the effects of extracellular AS on microglial cells and propose autophagy as a rescue mechanism activated to restore lysosomal quality control after fAS-induced organelle rupture. We anticipate that further studies evaluating the molecular mechanisms triggered by protein

Journal of Cell Science (2018) 131, jcs226241. doi:10.1242/jcs.226241

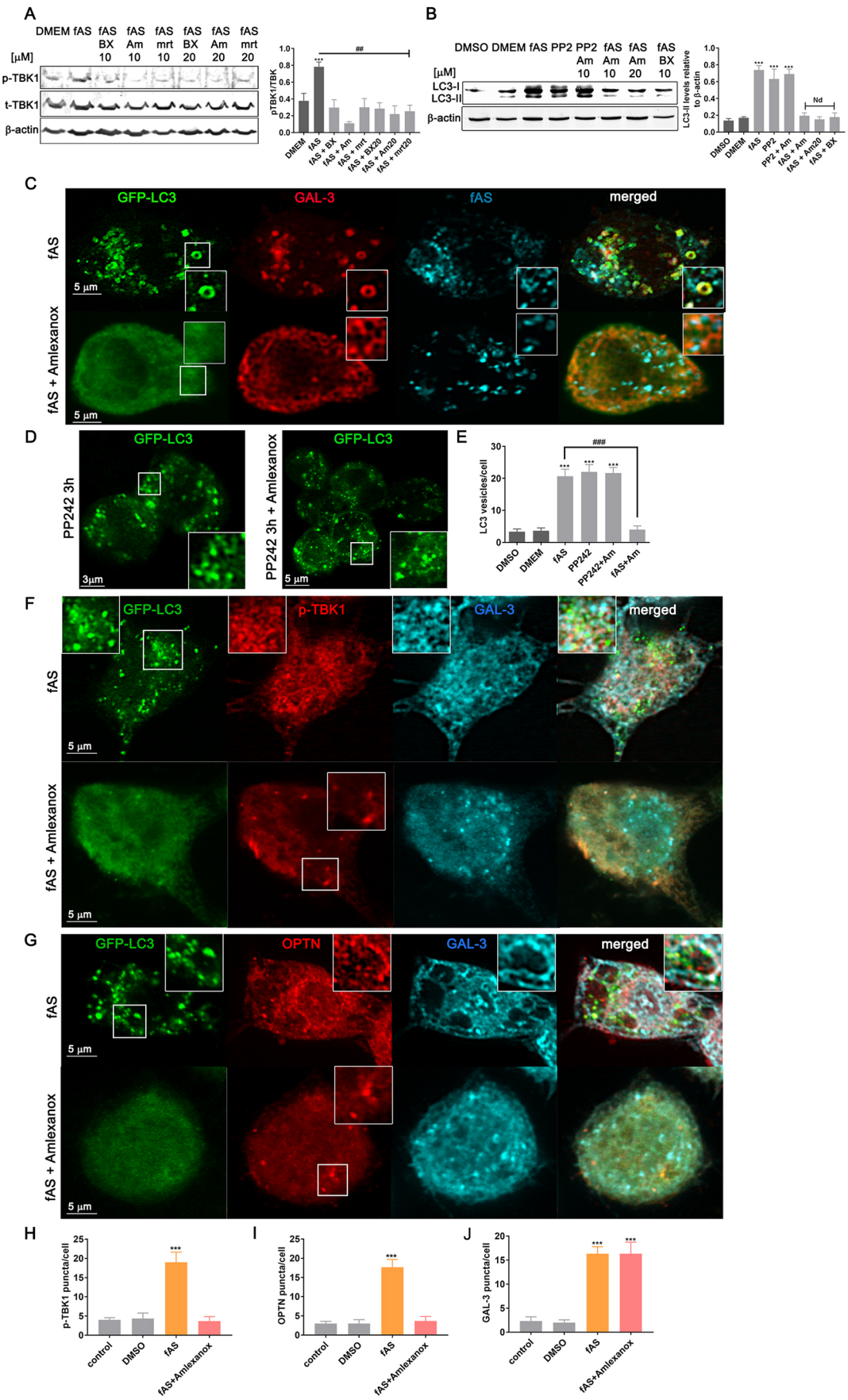

Fig. 7. See next page for legend.

Journal of Cell Science

Fig. 7. Effects of TBK1 inhibition on LC3 and autophagy adaptors recruitment to damaged lysosomes after fAS stimulation. (A) BV2 cells were pre-treated with the TBK1 inhibitors BX795 (BX), Amlexanox (Am) and MRT67307 (mrt) for 1 h or left untreated. Next, microglial cells were stimulated with fAS for 12 h and cells lysates were examined using western immunoblotting. The bar graph shows mean±s.e.m. relative densitometry quantification of phosphorylated (p) and total TBK1 bands. (B) BV2 cells pre-treated with Amlexanox or BX795 for 1 h were stimulated with PP242 (PP2, 1 µM) and fAS (5 µM) for 3 h and 12 h, respectively. Cell lysates were collected and analysed using western immunoblotting. The bar graph shows mean±s.e.m. densitometry quantification of LC3-II relative to β-actin bands. (C–E) BV2 GFP–LC3 cells treated with Amlexanox or left untreated were stimulated with fAS (5 µM, 12 h) (C) or PP242 (1 µM, 3 h) (D). fAS-stimulated microglial cells in C were also stained for GAL-3 to reveal LC3/GAL-3 co-localisation. (E) Quantification of mean±s.e.m. LC3 puncta for the indicated conditions using ImageJ particle counting plugin. (F,G) BV2 GFP–LC3 cells treated and stimulated as described in C were fixed and stained for pTBK1 (F) or OPTN (red) (G) and GAL-3 (cyan). (H–J) Next, mean±s.e.m. pTBK1 (H), OPTN (I) and GAL-3 (J) puncta in F,G were quantified. Image crops show magnification of the selected areas (white box). Results from at least three independent experiments were analysed by one-way ANOVA followed by post-hoc Dunnet's test; n=3. ***P<0.001; ##P<0.01; ###P<0.001, fAS in comparison with fAS in the presence of TBK1 inhibitors as indicated; Nd, no significant difference.

aggregates and their crosstalk with the autophagy pathway not only in neurons, but also in glial cells, would shed light on novel therapeutic targets for neurodegenerative disorders.

MATERIALS AND METHODS

Reagents

Dulbecco's Modified Eagle Medium (DMEM), Opti-MEM, fetal bovine serum (FBS), penicillin, glutamine, G418, streptomycin, Silencer select FIP200 siRNA (4390771), Silencer select negative control 1 (4390843), Lipofectamine RNAiMAX (13778100) and LysoTracker Blue (L7525) were obtained from Thermo Fisher Scientific. Antibodies used for western blotting were rabbit polyclonal anti-LC3 (Sigma, L7543; 1:1000), mouse monoclonal anti-β-actin (Cell Signaling Technology, 8H10D10; 1:1000), rabbit polyclonal anti-Optineurin (Cayman, 100000; 1:1000), mouse monoclonal anti-TBK1 (Santa Cruz, 398366; 1:1000) and rabbit monoclonal anti-phosphoTBK1 (Cell Signaling Technology, 5483S; 1:1000). Antibodies used for immunofluorescence were rabbit monoclonal anti-LC3 A/B (Cell Signaling Technology, D3U4C; 1:100), rat monoclonal anti-LAMP-1 (BioLegend, 121601; 1:200), mouse monoclonal anti-galectin-3 (BioLegend, 125401; 1:300), rabbit polyclonal anti-GALNS (GeneTex, 110237; 1:100), rabbit polyclonal anti-Optineurin (Cayman, 100000; 1:100), mouse monoclonal anti-TBK1 (Santa Cruz, 398366; 1:100) and mouse monoclonal anti-Ubiquitin (Cell Signaling Technology, 3936S; 1:100). PP242 (13643) and BafA1 (11038) were purchased from Cayman. Spautin-1 (SML0440) was purchased from Sigma. MRT67307 (19916) and Amlexanox (14181) were purchased from Cayman. BX795 (HY-10514) was purchased from MedChemExpress. MitoSpy Green FM and MitoSpy Orange CMTMRos were obtained from BioLegend. Magic Red Cathepsin-B Kit was purchased from Bio-Rad. FITC Annexin V Apoptosis Detection Kit was purchased from Becton Dickinson.

Cell culture and transfections

The murine microglial cell line BV2 was a kind gift from Dr Dennis J. Selkoe (Harvard Medical School, Center for Neurological Diseases, Brigham and Women's Hospital, Boston, MA, USA). The cells were grown in DMEM supplemented with 10% heat-inactivated FCS, 2 mM glutamine and 100 µg/ml streptomycin and maintained at 37°C and 5% CO_2.

For stable GFP-LC3 expression, BV2 cells were transduced with pBabe-GFP-LC3 retrovirus generated as previously described (Florey et al., 2011). Cells were selected with 10 µg/ml blasticidin for 4 days. BV2 stably transfected with ATG13 were cultured in media identical in composition to wild-type media, except for the addition of 400 µg/ml G418. BV2 cells were transfected with X-tremeGENE HP DNA Transfection Reagent (Roche, 06366236001) following manufacturer's indications. CFP–LC3 plasmid was a kind gift from Dr Tamotsu Yoshimori (Osaka University Graduate School of Medicine, Osaka, Japan). Silencer Select FIP200 (Thermo Fisher, 4390771) and negative control siRNAs (Thermo Fisher, 4390843) solutions were prepared according to the manufacturer's instructions and experiments were performed 48 h after transfection. Lipofectamine RNAiMAX (Thermo Fisher, 13778100) was used as transfection reagent.

Isolation of primary microglial cells from adult mice

After perfusion with PBS, brains from 6- to 8-week-old mice C57BL/6J (15 mice/group) were collected in DMEM, dispersed with scissors, resuspended in PBS containing 0.3% collagenase D (Roche) and 10 mM HEPES buffer (Invitrogen), and incubated for 30 min at 37°C. Brain homogenates were then filtered in 70 µm-pore cell strainers (Becton Dickinson), centrifuged (7 min, 300 ***g***), washed, and resuspended in 70% isotonic Percoll (GE Healthcare). Cell suspension (3.5 ml) was transferred to 15 ml polypropylene conical tubes, layered over 5 ml of 25% isotonic Percoll, and then overlaid with 3 ml of PBS. After centrifugation (30 min, 800 ***g***, 4°C), the 70%:25% Percoll interphase layers were collected, and the cells were washed in DMEM. Finally, the adherent cells, which contained 90% of CD11b+ cells, were cultured in DMEM supplemented with 10% heat-inactivated FCS, 2 mM glutamine, 100 U/ml penicillin, 100 µg/ml streptomycin, 100 µg/ml sodium pyruvate and 10 mM HEPES buffer (Invitrogen). Microglial cells were washed with PBS and resuspended in medium containing 10% heat-inactivated FCS, alpha-synuclein or other stimuli and then cultured for the indicated times at 37°C. Morphological changes were observed using a contrast phase microscope. Animal care was provided in accordance with the procedures outlined in the National Institutes of Health (NIH) Guide for the Care and Use of Laboratory Animals (Publication 86-23, 1985). The experimental protocols were approved by the Institutional Animal Care and Use Committee of Centro de Investigaciones en Bioquímica Clínica e Inmunología (CIBICI), Consejo Nacional de Investigaciones Científicas y Técnicas (CONICET). Our animal facility obtained NIH animal welfare assurance (assurance A5802-01, Office of Laboratory Animal Welfare, NIH, Bethesda, MD, USA).

Cell culture treatments

BV2 cells were grown in six-well plates to 65–70% confluence (for immunofluorescence) or 70–80% confluence (for western blotting) before treatments. Primary microglial cells were grown in chamber slides or 48-well plates to 65–70% confluence before treatments. AS fibrils and monomers were added at 1 µM at indicated time points. PP242 was used at 1 µM for 3 h. Mammalian PI3KC3 was blocked by the addition of spautin-1 (10 µM) for 24 h before stimulation. TBK1 was inhibited by the addition of BX795 (1 µM), MRT67307 (1 µM) or Amlexanox (1 µM) for 1 h before stimulation. Autophagosome maturation was blocked using BAF, at a final concentration of 200 nM, in normal growth medium for 1 h, unless otherwise stated.

Preparation of monomeric and aggregated AS

Monomeric AS stock solutions were prepared in PBS buffer and 0.02% sodium azide and centrifuged (14,100 ***g***, 30 min) before use in order to remove possible aggregates. After that, solutions were sterilised by filtration (22 µm pore size). Protein concentration was determined by absorbance using an ε275 of 5600 M^{-1} cm^{-1}. Fibrillation was achieved by incubating 400 µM monomeric AS stock solutions at 70°C and 800 rpm in a Thermomixer 5436 orbital shaker (Eppendorf), conditions that lead to faster aggregation kinetics (Celej et al., 2012). Fibril formation was monitored using the thioflavin T (ThioT) fluorescence assay. Fibrils were isolated by three consecutive cycles of centrifugation (14,000 ***g***, 30 min) and resuspended in PBS buffer. Protein concentrations in monomeric units were determined using the absorbance of aliquots incubated in 6 M guanidinium chloride at 25°C for 24 h. Endotoxin levels were evaluated by use of the Limulus Amebocyte Lysate (LAL) assay, and endotoxin content was lower than detection limit (<0.24 EU/ml). AS protein labelling: AS fibrils were conjugated by using Alexa Fluor 647 (Molecular Probes, A2006) or Alexa Fluor 546 (Molecular Probes, A2004) NHS Ester dye according to manufacturer's instructions.

Journal of Cell Science (2018) 131, jcs226241. doi:10.1242/jcs.226241

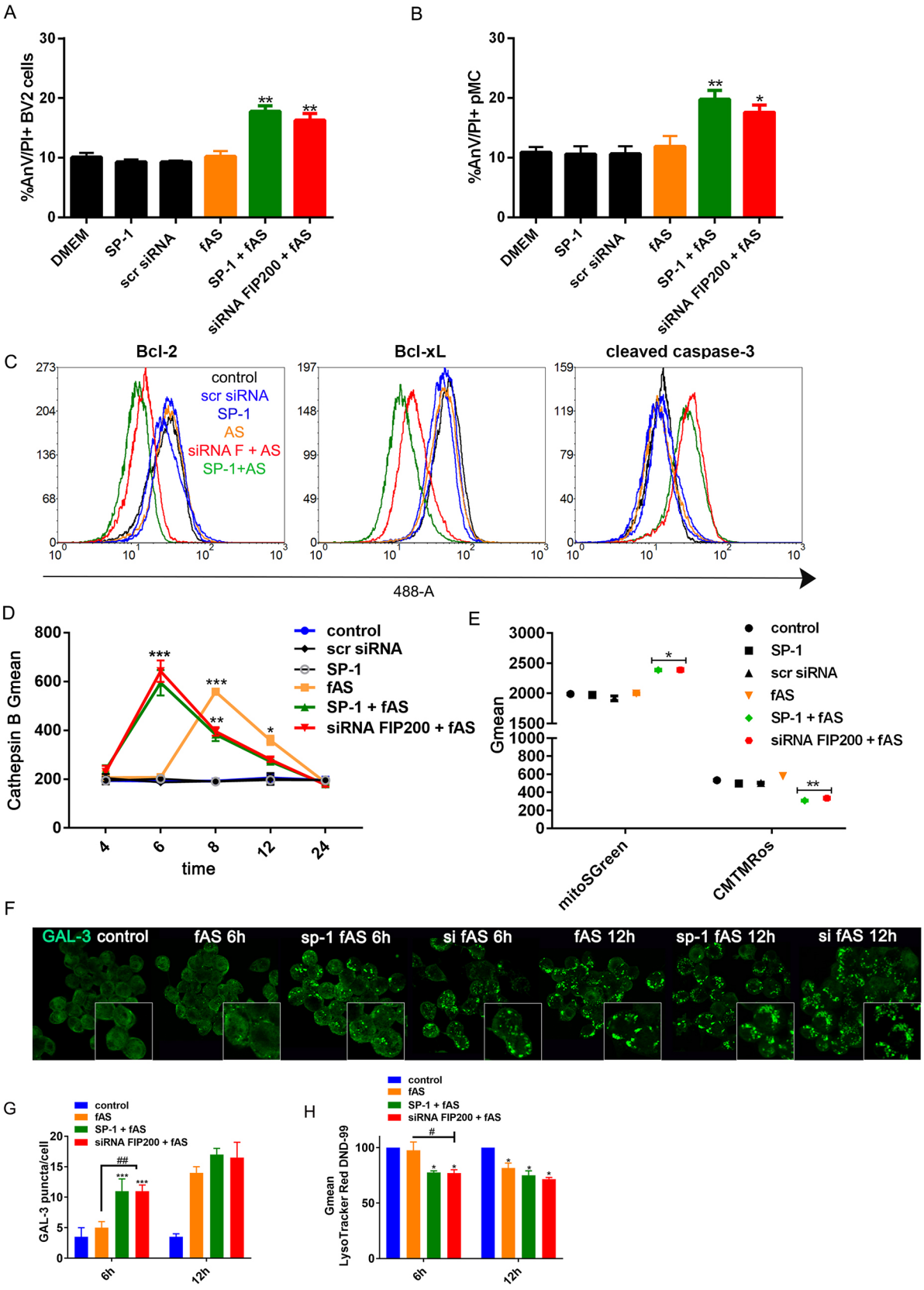

Fig. 8. See next page for legend.

The label density of the fluorophore in the fibril preparation was 5% to ensure a negligible effect on the fibril structure. We carefully checked the ultrastructure (TEM) (Fig. S5D), tinctorial properties (ThioT) and secondary structure features (IR) of labelled fibrils and compare them with unlabelled wild-type fibrils. We did not observe any difference in the properties assayed.

Fig. 8. Effects of fAS stimulation on cathepsin-B activity, mitochondrial quality and microglial cell survival after autophagy inhibition. (A,B) BV2 (A) or primary (B) microglial cells were left untreated or treated with spautin-1 (10 µM) for 24 h or FIP200 siRNA for 48 h. Cells were then stimulated with fAS (5 µM) for 24 h and cell death was evaluated using propidium iodide (PI) combined with Annexin V–FITC staining and subsequent flow cytometric analysis. Mean±s.e.m. percentages of Annexin V–FITC/IP double-positive dead cells are shown. (C) BV2 microglial cells were treated and stimulated as described in A and BCL-2, BCL-xL and cleaved caspase-3 protein levels were evaluated using flow cytometry. Graphs show representative histograms for each protein. (D,E) BV2 microglial cells were left untreated or treated with spautin-1 (SP-1, 10 µM) for 24 h or FIP200 siRNA for 48 h and stimulated with fAS (5 µM) for 24 h. Untreated (control) and scramble (scr) siRNA as controls also shown. Cathepsin-B activity (D) and mitochondrial mass and membrane potential (E) were measured as described in Fig. 5H and I, respectively. (F–H) BV2 cells were treated with the autophagy inhibitors spautin-1 (SP-1, 10 µM) for 24 h or FIP200 siRNA for 48 h (si) and stimulated with fAS (5 µM) at the indicated time points. (F) GAL-3 immunostaining. (G,H) Mean±s.e.m. quantification of GAL-3 puncta (G) and LysoTracker Red DND-99 staining (H). LysoTracker staining was evaluated using flow cytometry and results are relative to the mean fluorescence intensity (Gmean) of the control condition. Results were analysed by one-way ANOVA followed by post-hoc Dunnet's test; n=3. *P<0.05, **P<0.01, ***P<0.001; $^{\#}P$<0.05, $^{\#\#}P$<0.01 when comparing fAS with fAS plus SP-1 or FIP200 siRNA treatment.

Western immunoblotting

After treatment with AS fibrils or monomers, 2×106 BV2 microglial cells were harvested by centrifugation at indicated time points. After washing with PBS, cells were lysed using RIPA Lysis Buffer (89900, Thermo Fisher). Subsequently, cell lysates were sonicated and boiled. Proteins were electrophoresed on 12% SDS-PAGE gel under reducing conditions and transferred on to Immun-Blot PVDF Membrane (Bio-Rad). The membranes were blocked with 5% nonfat milk and 0.1% Tween-20 in TBS for 2 h at room temperature and then were incubated with primary antibodies overnight at 4°C. Then, membranes were incubated with secondary antibodies (IRDye, LI-COR Biosciences; 1:15,000) for 1 h and 30 min at room temperature and protein bands were detected with an Odyssey Infrared Imaging System (LI-COR Biosciences).

Immunofluorescence assays

Following the appropriated treatments, BV2 cells grown on glass coverslips in 6-well plates, or primary microglial cells grown on Lab-Tek chamber slides (Thermo Fisher), were fixed with 100% ice-cold methanol for 10 min on ice. The cells were then blocked for a minimum of 1 h in 5% (w/v) BSA/PBS before staining with the appropriate primary antibodies. After three rinses with PBS, samples were incubated with Alexa Fluor 488 or Alexa Fluor 546 secondary antibodies (A11008, A11081, Invitrogen; 1:750) for 60 min. The slides were analysed under a laser scanning confocal fluorescence microscope (Olympus FV1000) or under a wide-field fluorescence microscope (Leica DMi8). For the galectin puncta assay, staining for immunofluorescence and image analysis were done following a previously characterised protocol (Aits et al., 2015). Briefly, BV2 or primary microglial cells were incubated in the presence or the absence of fibrillar AS and immunolabelled with a monoclonal rat anti-mouse galectin-3 antibody (BioLegend, 125402; 1:300). Alternatively, immunostaining with a monoclonal rat anti-mouse galectin-3 Alexa Fluor 488-conjugated antibody (BioLegend, 125410; 1:400) was also performed. Next, fluorescence images were acquired under a wide-field or laser-scanning confocal fluorescence microscope and galectin-3 puncta formation was followed over time. Incubation for 2 h at 37°C with a 500 µM solution of LLOME crystals was used as positive control for lysosomal damage. Spatial deconvolution, 3D surface-rendered images and 3D surface-rendered movies were created with SVI Huygens Software. Image processing and analysis were performed using Fiji open source software (Schindelin et al., 2012). Co-localisation analyses were performed after z-stack deconvolution by using SVI Huygens Software. LC3, GAL-3, pTBK1, OPTN and ubiquitin puncta quantification in BV2 cells was done after analysis of at least four different fields with 15–20 cells each. For experiments with primary cells, at least 20 cells were analysed per condition. Statistical analyses show mean±s.e.m. of three independent experiments.

Live-cell imaging

Live-cell imaging was performed in cells that had been plated onto 22 mm diameter coverslips (BDH) and transiently transfected with the relevant constructs. Individual coverslips were placed in an imaging chamber with 2 ml of medium and the appropriate treatment. LysoTracker Blue (Thermo Fisher, L7525; 1:10,000), where stated, was added to samples 30 min before imaging began. Samples were then placed in a Solent environment chamber (Solent Scientific, custom made) before mounting on the microscope, all at 37°C. Wide-field imaging experiments were performed on a Nikon Ti-E-based system. The Nikon Ti-E-based system comprised a Nikon Ti-E microscope, 100×1.4 N.A. objective (Nikon), SpecraX LED illuminator (Lumencor), 410/504/582/669-Di01 and Di01-R442/514/561 dichroic mirrors (Semrock), Hamamatsu Flash 4.0 sCMOS camera, emission filter wheel (Sutter Instruments) and was controlled using Nikon Elements software. Excitation (ex) and emission (em) filters (all from Semrock) were as follows: CFP 434/17 (ex) 480/17 (em), GFP 480/10 (ex) 525/30 (em), mRFP 560/25 (ex) 607/36 (em).

Live-cell imaging videos were analysed with Fiji as previously described (Karanasios and Ktistakis, 2015; Karanasios et al., 2016). In brief, montages of independent events were created from the captured videos. We consider as an independent event all the frames that correspond to the formation and collapse of GFP–LC3, GFP–ATG13 or CFP–LC3 particles (as stated in Fig. S2C), starting and finishing with the frames in which the fluorescence of the particle is clearly above the background fluorescence. Frames corresponding to time points before the beginning or after the end of a particular event were carefully scanned, and events corresponding to particles moving out of focus and then back in were excluded from the analysis. For the analysis of the distance among GFP–LC3, CFP–LC3 or GFP–ATG13 and the different markers, the same coordinates were used to create montages of the other markers and composite images of the two channels were created to analyse the co-localisation of the two proteins. Lines were drawn crossing the sites of closest association (judged by eye in large magnification) and line plots of the fluorescence intensity were used to decide on association. Association was scored when the same pixels had signal above the background for both channels and the mean of association scores (expressed as percentages) was calculated. At least 50 montages were used for analysis.

Correlative light-electron microscopy (CLEM) experiments

For wide-field electron microscopy correlation assays, BV2 GFP–LC3 cells were cultured on 3 mm carbon-coated sapphire discs and stimulated with labelled AS (3 µM) for 12 h. High-pressure freezing, ultrathin sectioning for electron microscopy, image acquisition and correlation analysis were done as described previously (Kukulski et al., 2012). Briefly, after cellular stimulation, microglial cells were high-pressure frozen using an Abra Fluid HPM-010 and transferred to the automated freeze substitution apparatus (Leica EM AFS2) under liquid nitrogen. Semi-thick 300 nm sections were prepared using a Leica UC6 or UF6 ultramicrotome and picked up on finder 200-mesh copper grids coated with carbon. Next, immunofluorescence images were acquired using an Olympus ScanR microscope. Previous to the EM acquisition, colloidal gold particles, 10 nm in diameter, were placed on top of the sections to serve as fiducial markers for alignment of the tomograms. Tilt series were acquired using a FEI Tecnai F30 microscope operating at 300 kV with a Gatan OneView camera at a binned (2) pixel size of 1.25 nm using SerialEM (Mastronarde, 2005). Images were recorded at 1° intervals over a tilt range of +60° to −60°. Electron and fluorescent image overlays were obtained by using ec-CLEM plugin (Paul-Gilloteaux et al., 2017) from ICY software (de Chaumont et al., 2012). IMOD software package (Kremer et al., 1996) was used to create 3D reconstructions from the tilt series and to create 3D models of the autophagosomes and membranes. At least three different grids with 15–25 cells each and two or more regions of interest per cell were acquired per condition.

For live-cell CLEM assays, BV2 GFP–LC3 cells were grown on a gridded cell-culture dish (MatTek) and live-imaged using wide-field microscopy using a Zeiss Celldiscoverer 7 microscope after 12 h of AS stimulation. A bright field image of the area containing the cell of interest was acquired at low magnification to visualise the grid and therefore precisely localise the position of the cell. Cells were fixed in 2.5%

glutaraldehyde (GA, Electron Microscopy Sciences) in 0.1 M cacodylate buffer immediately after detecting the event of interest. The subsequent EM processing steps (OSO4, UA, dehydration) were performed using a PELCO Biowave Pro microwave processor (Ted Pella). After dehydration, the coverslip was detached from the MatTek dish and put on an Epon-filled capsule. Following polymerisation, the area containing the cell of interest was retrieved by means of the grid coordinate system that remained impressed on the block surface. The blocks were then sectioned with a Leica UC7 ultramicrotome and 300 nm sections were collected on formvar-coated slot grids. Tilt series of the cell of interest were acquired with a FEI Tecnai F30 electron microscope. Tomogram reconstruction, segmentation and 3D rendering was carried out with the IMOD software package (Kremer et al., 1996).

Evaluation of mitochondrial quality, cathepsin-B activity and LysoTracker staining

BV2 microglial cells were left untreated or stimulated with fibrillar AS from 8 to 48 h. Next, the cells were harvested, washed twice with fresh medium and incubated for 30 min at 37°C in DMEM supplemented with 10% heat-inactivated FCS containing the following dyes: 100 nM MitoSpy Green FM (BioLegend, 424805) to measure mitochondrial mass, 100 nM MitoSpy Orange CMTMRos (BioLegend, 424803) to measure mitochondrial membrane potential and 26× Magic Red Cathepsin-B substrate (Bio-Rad, ICT937) to measure cathepsin-B activity. LysoTracker Red DND-99 staining (Invitrogen, L7528) was done following manufacturer instructions and the status of acidified organelles assessed by quantification of LysoTracker Red DND-99 fluorescence intensity using flow cytometry. In all cases, cells were washed and resuspended in 300 µl of FACS buffer before acquisition. Flow cytometric analyses were performed on a FACSCanto II cytometer (Becton Dickinson) using FCS Express (De Novo Software.

Evaluation of cell death using flow cytometry

BV2 microglial cells and primary microglial cells were washed twice with PBS and incubated with propidium iodide (PI) for 2 min in 300 µl of FACS buffer. For annexin V (AnV) and PI dual staining, the cells were harvested, washed twice with binding buffer, and incubated with FITC-conjugated AnV and PI following manufacturer instructions (FITC Annexin V Apoptosis Detection Kit, Becton Dickinson). For Bcl-2, Bcl-xL and cleaved caspase-3 staining, BV2 cells were fixed and permeabilised by using Cytofix/Cytoperm kit (Becton Dickinson) and incubated with the monoclonal primary antibodies (Cell Signaling Technology). After 1 h, cells were washed and incubated for 30 min with an anti-rabbit Alexa Fluor 488 antibody (A-11008, Invitrogen; 1:400). Next, cells were washed with PBS and resuspended in 300 µl of FACS buffer. Microglial cells were then analysed using flow cytometry on a FACSCanto II cytometer using FCS Express software.

Statistical analyses

The results were analysed using one-way analysis of variance (ANOVA) model, as indicated for every experiment. GraphPad Prism 6.0 was used to carry out the computations for all analyses. Results represent mean±s.e.m. of at least three experiments. Statistical significance was defined as $P \leq 0.05$.

Acknowledgements

C.B. thanks EMBO, EMBL, Boehringer Ingelheim Fonds, IUBMB Wood-Whelan Fellowship and The Company of Biologists Travelling Fellowships for supporting short-research stays abroad. The authors would like to thank the Center of Micro and Nanoscopy of Cordoba (Cordoba, Argentina), the Imaging Facility at Babraham Institute (Cambridge, UK) and the Electron Microscopy Core Facility at EMBL (Heidelberg, Germany) for their technical assistance and helpful advice. We thank M. P. Abadie, M. P. Crespo, C. Mas, C. Sampedro, F. Navarro, D. Lutti, C. Florit, P. Icely and V. Blanco for their excellent technical assistance.

Competing interests

The authors declare no competing or financial interests.

Author contributions

Conceptualisation: C.B., P.I.; Methodology: C.B., J.M.P.R., D.S.A., J.I.G., P.R., A.K., M.S.C., Y.S., N.T.K.; Software: C.B.; Formal analysis: C.B., J.I.G., P.R.; Investigation: C.B., J.M.P.R., N.T.K., P.I.; Resources: D.S.A., J.I.G., P.R., A.K., J.M.W., O.F., M.S.C., Y.S., P.I.; Writing - original draft: C.B., P.I.; Writing - review & editing: C.B., J.M.P.R., N.T.K., P.I.; Supervision: N.T.K., P.I.; Project administration: P.I.; Funding acquisition: P.I.

Funding

This work was supported in part by Fondo para la Investigación Científica y Tecnológica (FONCyT) (PRESTAMO BID PICT 2014 2961) Argentina, Consejo Nacional de Investigaciones Científicas y Técnicas (CONICET) and Secretaria de Ciencia y Tecnología - Universidad Nacional de Córdoba (SECyT-UNC), Argentina. Its contents are solely the responsibility of the authors and do not necessarily represent the official views of FONCyT, CONICET and SECyT-UNC.

Supplementary information

Supplementary information available online at
http://jcs.biologists.org/lookup/doi/10.1242/jcs.226241.supplemental

References

Aits, S. and Jaattela, M. (2013). Lysosomal cell death at a glance. *J. Cell Sci.* **126**, 1905-1912.

Aits, S., Kricker, J., Liu, B., Ellegaard, A.-M., Hämälistö, S., Tvingsholm, S., Corcelle-Termeau, E., Høgh, S., Farkas, T., Holm Jonassen, A. et al. (2015). Sensitive detection of lysosomal membrane permeabilization by lysosomal galectin puncta assay. *Autophagy* **11**, 1408-1424.

Arroyo, D. S., Soria, J. A., Gaviglio, E. A., Garcia-Keller, C., Cancela, L. M., Rodriguez-Galan, M. C., Wang, J. M. and Iribarren, P. (2013). Toll-like receptor 2 ligands promote microglial cell death by inducing autophagy. *FASEB J.* **27**, 299-312.

Asai, H., Ikezu, S., Tsunoda, S., Medalla, M., Luebke, J., Haydar, T., Wolozin, B., Butovsky, O., Kügler, S. and Ikezu, T. (2015). Depletion of microglia and inhibition of exosome synthesis halt tau propagation. *Nat. Neurosci.* **18**, 1584-1593.

Axe, E. L., Walker, S. A., Manifava, M., Chandra, P., Roderick, H. L., Habermann, A., Griffiths, G. and Ktistakis, N. T. (2008). Autophagosome formation from membrane compartments enriched in phosphatidylinositol 3-phosphate and dynamically connected to the endoplasmic reticulum. *J. Cell Biol.* **182**, 685-701.

Bir, A., Sen, O., Anand, S., Khemka, V. K., Banerjee, P., Cappai, R., Sahoo, A. and Chakrabarti, S. (2014). alpha-Synuclein-induced mitochondrial dysfunction in isolated preparation and intact cells: implications in the pathogenesis of Parkinson's disease. *J. Neurochem.* **131**, 868-877.

Bisht, K., Sharma, K. P., Lecours, C., Sánchez, M. G., El Hajj, H., Milior, G., Olmos-Alonso, A., Gómez-Nicola, D., Luheshi, G., Vallières, L. et al. (2016). Dark microglia: a new phenotype predominantly associated with pathological states. *Glia* **64**, 826-839.

Bourdenx, M., Bezard, E. and Dehay, B. (2014). Lysosomes and alpha-synuclein form a dangerous duet leading to neuronal cell death. *Front. Neuroanat.* **8**, 83.

Bussi, C., Peralta Ramos, J. M., Arroyo, D. S., Gaviglio, E. A., Gallea, J. I., Wang, J. M., Celej, M. S. and Iribarren, P. (2017). Autophagy down regulates pro-inflammatory mediators in BV2 microglial cells and rescues both LPS and alpha-synuclein induced neuronal cell death. *Sci. Rep.* **7**, 43153.

Celej, M. S., Sarroukh, R., Goormaghtigh, E., Fidelio, G. D., Ruysschaert, J.-M. and Raussens, V. (2012). Toxic prefibrillar α-synuclein amyloid oligomers adopt a distinctive antiparallel β-sheet structure. *Biochem. J.* **443**, 719-726.

Chang, C., Lang, H., Geng, N., Wang, J., Li, N. and Wang, X. (2013). Exosomes of BV-2 cells induced by alpha-synuclein: important mediator of neurodegeneration in PD. *Neurosci. Lett.* **548**, 190-195.

Cirman, T., Orešić, K., Mazovec, G. D., Turk, V., Reed, J. C., Myers, R. M., Salvesen, G. S. and Turk, B. (2004). Selective disruption of lysosomes in HeLa cells triggers apoptosis mediated by cleavage of Bid by multiple papain-like lysosomal cathepsins. *J. Biol. Chem.* **279**, 3578-3587.

Codolo, G., Plotegher, N., Pozzobon, T., Brucale, M., Tessari, I., Bubacco, L. and de Bernard, M. (2013). Triggering of inflammasome by aggregated alpha-synuclein, an inflammatory response in synucleinopathies. *PLoS ONE* **8**, e55375.

de Chaumont, F., Dallongeville, S., Chenouard, N., Hervé, N., Pop, S., Provoost, T., Meas-Yedid, V., Pankajakshan, P., Lecomte, T., Le Montagner, Y. et al. (2012). Icy: an open bioimage informatics platform for extended reproducible research. *Nat. Methods* **9**, 690-696.

Degenhardt, K., Mathew, R., Beaudoin, B., Bray, K., Anderson, D., Chen, G., Mukherjee, C., Shi, Y., Gélinas, C., Fan, Y. et al. (2006). Autophagy promotes tumor cell survival and restricts necrosis, inflammation, and tumorigenesis. *Cancer Cell* **10**, 51-64.

Di Maio, R., Barrett, P. J., Hoffman, E. K., Barrett, C. W., Zharikov, A., Borah, A., Hu, X., McCoy, J., Chu, C. T., Burton, E. A. et al. (2016). alpha-Synuclein binds to TOM20 and inhibits mitochondrial protein import in Parkinson's disease. *Sci. Transl. Med.* **8**, 342ra78.

Droga-Mazovec, G., Bojič, L., Petelin, A., Ivanova, S., Romih, R., Repnik, U., Salvesen, G. S., Stoka, V., Turk, V. and Turk, B. (2008). Cysteine cathepsins trigger caspase-dependent cell death through cleavage of bid and antiapoptotic Bcl-2 homologues. *J. Biol. Chem.* **283**, 19140-19150.

Dunn, W. A. Jr. (1990a). Studies on the mechanisms of autophagy: formation of the autophagic vacuole. *J. Cell Biol.* **110**, 1923-1933.
Dunn, W. A. Jr. (1990b). Studies on the mechanisms of autophagy: maturation of the autophagic vacuole. *J. Cell Biol.* **110**, 1935-1945.
Dupont, N., Nascimbeni, A. C., Morel, E. and Codogno, P. (2017). Molecular mechanisms of noncanonical autophagy. *Int. Rev. Cell Mol. Biol.* **328**, 1-23.
Esteves, A. R., Arduino, D. M., Silva, D. F. F., Oliveira, C. R. and Cardoso, S. M. (2011). Mitochondrial dysfunction: the road to alpha-synuclein oligomerization in PD. *Parkinsons Dis.* **2011**, 693761.
Flavin, W. P., Bousset, L., Green, Z. C., Chu, Y., Skarpathiotis, S., Chaney, M. J., Kordower, J. H., Melki, R. and Campbell, E. M. (2017). Endocytic vesicle rupture is a conserved mechanism of cellular invasion by amyloid proteins. *Acta Neuropathol.* **134**, 629-653.
Florey, O., Kim, S. E., Sandoval, C. P., Haynes, C. M. and Overholtzer, M. (2011). Autophagy machinery mediates macroendocytic processing and entotic cell death by targeting single membranes. *Nat. Cell Biol.* **13**, 1335-1343.
Frake, R. A., Ricketts, T., Menzies, F. M. and Rubinsztein, D. C. (2015). Autophagy and neurodegeneration. *J. Clin. Invest.* **125**, 65-74.
Freeman, D., Cedillos, R., Choyke, S., Lukic, Z., McGuire, K., Marvin, S., Burrage, A. M., Sudholt, S., Rana, A., O'Connor, C. et al. (2013). Alpha-synuclein induces lysosomal rupture and cathepsin dependent reactive oxygen species following endocytosis. *PLoS ONE* **8**, e62143.
Green, D. R. and Levine, B. (2014). To be or not to be? How selective autophagy and cell death govern cell fate. *Cell* **157**, 65-75.
Hara, T., Nakamura, K., Matsui, M., Yamamoto, A., Nakahara, Y., Suzuki-Migishima, R., Yokoyama, M., Mishima, K., Saito, I., Okano, H. et al. (2006). Suppression of basal autophagy in neural cells causes neurodegenerative disease in mice. *Nature* **441**, 885-889.
Hara, T., Takamura, A., Kishi, C., Iemura, S., Natsume, T., Guan, J.-L. and Mizushima, N. (2008). FIP200, a ULK-interacting protein, is required for autophagosome formation in mammalian cells. *J. Cell Biol.* **181**, 497-510.
Hayashi-Nishino, M., Fujita, N., Noda, T., Yamaguchi, A., Yoshimori, T. and Yamamoto, A. (2009). A subdomain of the endoplasmic reticulum forms a cradle for autophagosome formation. *Nat. Cell Biol.* **11**, 1433-1437.
Hoffmann, A., Ettle, B., Bruno, A., Kulinich, A., Hoffmann, A.-C., von Wittgenstein, J., Winkler, J., Xiang, W. and Schlachetzki, J. C. M. (2016). Alpha-synuclein activates BV2 microglia dependent on its aggregation state. *Biochem. Biophys. Res. Commun.* **479**, 881-886.
Jo, C., Gundemir, S., Pritchard, S., Jin, Y. N., Rahman, I. and Johnson, G. V. W. (2014). Nrf2 reduces levels of phosphorylated tau protein by inducing autophagy adaptor protein NDP52. *Nat. Commun.* **5**, 3496.
Karanasios, E. and Ktistakis, N. T. (2015). Live-cell imaging for the assessment of the dynamics of autophagosome formation: focus on early steps. *Methods* **75**, 54-60.
Karanasios, E., Walker, S. A., Okkenhaug, H., Manifava, M., Hummel, E., Zimmermann, H., Ahmed, Q., Domart, M.-C., Collinson, L. and Ktistakis, N. T. (2016). Autophagy initiation by ULK complex assembly on ER tubulovesicular regions marked by ATG9 vesicles. *Nat. Commun.* **7**, 12420.
Kim, C., Ho, D.-H., Suk, J.-E., You, S., Michael, S., Kang, J., Joong Lee, S., Masliah, E., Hwang, D., Lee, H.-J. et al. (2013). Neuron-released oligomeric alpha-synuclein is an endogenous agonist of TLR2 for paracrine activation of microglia. *Nat. Commun.* **4**, 1562.
Komatsu, M., Waguri, S., Chiba, T., Murata, S., Iwata, J.-I., Tanida, I., Ueno, T., Koike, M., Uchiyama, Y., Kominami, E. et al. (2006). Loss of autophagy in the central nervous system causes neurodegeneration in mice. *Nature* **441**, 880-884.
Korac, J., Schaeffer, V., Kovacevic, I., Clement, A. M., Jungblut, B., Behl, C., Terzic, J. and Dikic, I. (2013). Ubiquitin-independent function of optineurin in autophagic clearance of protein aggregates. *J. Cell Sci.* **126**, 580-592.
Kremer, J. R., Mastronarde, D. N. and McIntosh, J. R. (1996). Computer visualization of three-dimensional image data using IMOD. *J. Struct. Biol.* **116**, 71-76.
Ktistakis, N. T. and Tooze, S. A. (2016). Digesting the expanding mechanisms of autophagy. *Trends Cell Biol.* **26**, 624-635.
Ktistakis, N. T., Karanasios, E. and Manifava, M. (2014). Dynamics of autophagosome formation: a pulse and a sequence of waves. *Biochem. Soc. Trans.* **42**, 1389-1395.
Kukulski, W., Schorb, M., Welsch, S., Picco, A., Kaksonen, M. and Briggs, J. A. G. (2012). Precise, correlated fluorescence microscopy and electron tomography of lowicryl sections using fluorescent fiducial markers. *Methods Cell Biol.* **111**, 235-257.
Lee, H.-J., Bae, E.-J. and Lee, S.-J. (2014). Extracellular alpha–synuclein-a novel and crucial factor in Lewy body diseases. *Nat. Rev. Neurol.* **10**, 92-98.
Li, F., Xie, X., Wang, Y., Liu, J., Cheng, X., Guo, Y., Gong, Y., Hu, S. and Pan, L. (2016). Structural insights into the interaction and disease mechanism of neurodegenerative disease-associated optineurin and TBK1 proteins. *Nat. Commun.* **7**, 12708.
Liang, C.-C., Wang, C., Peng, X., Gan, B. and Guan, J.-L. (2010). Neural-specific deletion of FIP200 leads to cerebellar degeneration caused by increased neuronal death and axon degeneration. *J. Biol. Chem.* **285**, 3499-3509.
Liu, J., Xia, H., Kim, M., Xu, L., Li, Y., Zhang, L., Cai, Y., Norberg, H. V., Zhang, T., Furuya, T. et al. (2011). Beclin1 controls the levels of p53 by regulating the deubiquitination activity of USP10 and USP13. *Cell* **147**, 223-234.
Longhena, F., Faustini, G., Missale, C., Pizzi, M., Spano, P. F. and Bellucci, A. (2017). The contribution of alpha-synuclein spreading to Parkinson's disease synaptopathy. *Neural Plast.* **2017**, 5012129.
Loria, F., Vargas, J. Y., Bousset, L., Syan, S., Salles, A., Melki, R. and Zurzolo, C. (2017). alpha-Synuclein transfer between neurons and astrocytes indicates that astrocytes play a role in degradation rather than in spreading. *Acta Neuropathol.* **134**, 789-808.
Lumkwana, D., du Toit, A., Kinnear, C. and Loos, B. (2017). Autophagic flux control in neurodegeneration: progress and precision targeting-Where do we stand? *Prog. Neurobiol.* **153**, 64-85.
Maejima, I., Takahashi, A., Omori, H., Kimura, T., Takabatake, Y., Saitoh, T., Yamamoto, A., Hamasaki, M., Noda, T., Isaka, Y. et al. (2013). Autophagy sequesters damaged lysosomes to control lysosomal biogenesis and kidney injury. *EMBO J.* **32**, 2336-2347.
Maier, O., Marvin, S. A., Wodrich, H., Campbell, E. M. and Wiethoff, C. M. (2012). Spatiotemporal dynamics of adenovirus membrane rupture and endosomal escape. *J. Virol.* **86**, 10821-10828.
Martin, L. J., Pan, Y., Price, A. C., Sterling, W., Copeland, N. G., Jenkins, N. A., Price, D. L. and Lee, M. K. (2006). Parkinson's disease alpha-synuclein transgenic mice develop neuronal mitochondrial degeneration and cell death. *J. Neurosci.* **26**, 41-50.
Martinez, J., Almendinger, J., Oberst, A., Ness, R., Dillon, C. P., Fitzgerald, P., Hengartner, M. O. and Green, D. R. (2011). Microtubule-associated protein 1 light chain 3 alpha (LC3)-associated phagocytosis is required for the efficient clearance of dead cells. *Proc. Natl. Acad. Sci. USA* **108**, 17396-17401.
Martinez, J., Malireddi, R. K. S., Lu, Q., Cunha, L. D., Pelletier, S., Gingras, S., Orchard, R., Guan, J.-L., Tan, H., Peng, J. et al. (2015). Molecular characterization of LC3-associated phagocytosis reveals distinct roles for Rubicon, NOX2 and autophagy proteins. *Nat. Cell Biol.* **17**, 893-906.
Mastronarde, D. N. (2005). Automated electron microscope tomography using robust prediction of specimen movements. *J. Struct. Biol.* **152**, 36-51.
Mazzulli, J. R., Zunke, F., Isacson, O., Studer, L. and Krainc, D. (2016). alpha-Synuclein-induced lysosomal dysfunction occurs through disruptions in protein trafficking in human midbrain synucleinopathy models. *Proc. Natl. Acad. Sci. USA* **113**, 1931-1936.
McGlinchey, R. P. and Lee, J. C. (2015). Cysteine cathepsins are essential in lysosomal degradation of alpha-synuclein. *Proc. Natl. Acad. Sci. USA* **112**, 9322-9327.
Minowa-Nozawa, A., Nozawa, T., Okamoto-Furuta, K., Kohda, H. and Nakagawa, I. (2017). Rab35 GTPase recruits NDP52 to autophagy targets. *EMBO J.* **36**, 2790-2807.
Moore, A. S. and Holzbaur, E. L. F. (2016). Dynamic recruitment and activation of ALS-associated TBK1 with its target optineurin are required for efficient mitophagy. *Proc. Natl. Acad. Sci. USA* **113**, E3349-E3358.
Nikoletopoulou, V., Papandreou, M.-E. and Tavernarakis, N. (2015). Autophagy in the physiology and pathology of the central nervous system. *Cell Death Differ.* **22**, 398-407.
Nixon, R. A., Wegiel, J., Kumar, A., Yu, W. H., Peterhoff, C., Cataldo, A. and Cuervo, A. M. (2005). Extensive involvement of autophagy in Alzheimer disease: an immuno-electron microscopy study. *J. Neuropathol. Exp. Neurol.* **64**, 113-122.
Osellame, L. D. and Duchen, M. R. (2014). Quality control gone wrong: mitochondria, lysosomal storage disorders and neurodegeneration. *Br. J. Pharmacol.* **171**, 1958-1972.
Paul-Gilloteaux, P., Heiligenstein, X., Belle, M., Domart, M.-C., Larijani, B., Collinson, L., Raposo, G. and Salamero, J. (2017). eC-CLEM: flexible multidimensional registration software for correlative microscopies. *Nat. Methods* **14**, 102-103.
Peelaerts, W., Bousset, L., Van der Perren, A., Moskalyuk, A., Pulizzi, R., Giugliano, M., Van den Haute, C., Melki, R. and Baekelandt, V. (2015). alpha-Synuclein strains cause distinct synucleinopathies after local and systemic administration. *Nature* **522**, 340-344.
Ransohoff, R. M. (2016). How neuroinflammation contributes to neurodegeneration. *Science* **353**, 777-783.
Reilly, S. M., Chiang, S.-H., Decker, S. J., Chang, L., Uhm, M., Larsen, M. J., Rubin, J. R., Mowers, J., White, N. M., Hochberg, I. et al. (2013). An inhibitor of the protein kinases TBK1 and IKK-ε improves obesity-related metabolic dysfunctions in mice. *Nat. Med.* **19**, 313-321.
Repnik, U., Hafner Česen, M. and Turk, B. (2014). Lysosomal membrane permeabilization in cell death: concepts and challenges. *Mitochondrion* **19**, 49-57.
Sanchez-Guajardo, V., Tentillier, N. and Romero-Ramos, M. (2015). The relation between alpha-synuclein and microglia in Parkinson's disease: recent developments. *Neuroscience* **302**, 47-58.
Schindelin, J., Arganda-Carreras, I., Frise, E., Kaynig, V., Longair, M., Pietzsch, T., Preibisch, S., Rueden, C., Saalfeld, S., Cardona, A. et al. (2012). Fiji: an open-source platform for biological-image analysis. *Nat. Methods* **9**, 676-682.
Shamas-Din, A., Kale, J., Leber, B. and Andrews, D. W. (2013). Mechanisms of action of Bcl-2 family proteins. *Cold Spring Harb. Perspect. Biol.* **5**, a008714.

Sundblad, V., Croci, D. O. and Rabinovich, G. A. (2011). Regulated expression of galectin-3, a multifunctional glycan-binding protein, in haematopoietic and non-haematopoietic tissues. *Histol. Histopathol.* **26**, 247-265.

Tait, S. W. G. and Green, D. R. (2010). Mitochondria and cell death: outer membrane permeabilization and beyond. *Nat. Rev. Mol. Cell Biol.* **11**, 621-632.

Thurston, T. L. M., Wandel, M. P., von Muhlinen, N., Foeglein, A. and Randow, F. (2012). Galectin 8 targets damaged vesicles for autophagy to defend cells against bacterial invasion. *Nature* **482**, 414-418.

Uchimoto, T., Nohara, H., Kamehara, R., Iwamura, M., Watanabe, N. and Kobayashi, Y. (1999). Mechanism of apoptosis induced by a lysosomotropic agent, L-Leucyl-L-Leucine methyl ester. *Apoptosis* **4**, 357-362.

Wild, P., Farhan, H., McEwan, D. G., Wagner, S., Rogov, V. V., Brady, N. R., Richter, B., Korac, J., Waidmann, O., Choudhary, C. et al. (2011). Phosphorylation of the autophagy receptor optineurin restricts Salmonella growth. *Science* **333**, 228-233.

Xilouri, M., Brekk, O. R. and Stefanis, L. (2016). Autophagy and Alpha-synuclein: relevance to Parkinson's disease and related synucleopathies. *Mov. Disord.* **31**, 178-192.

Xiong, S., Mu, T., Wang, G. and Jiang, X. (2014). Mitochondria-mediated apoptosis in mammals. *Protein Cell* **5**, 737-749.

Yu, T., Yang, Y., Yin, D. Q., Hong, S., Son, Y.-J., Kim, J.-H. and Cho, J. Y. (2015). TBK1 inhibitors: a review of patent literature (2011-2014). *Expert Opin. Ther. Pat.* **25**, 1385-1396.

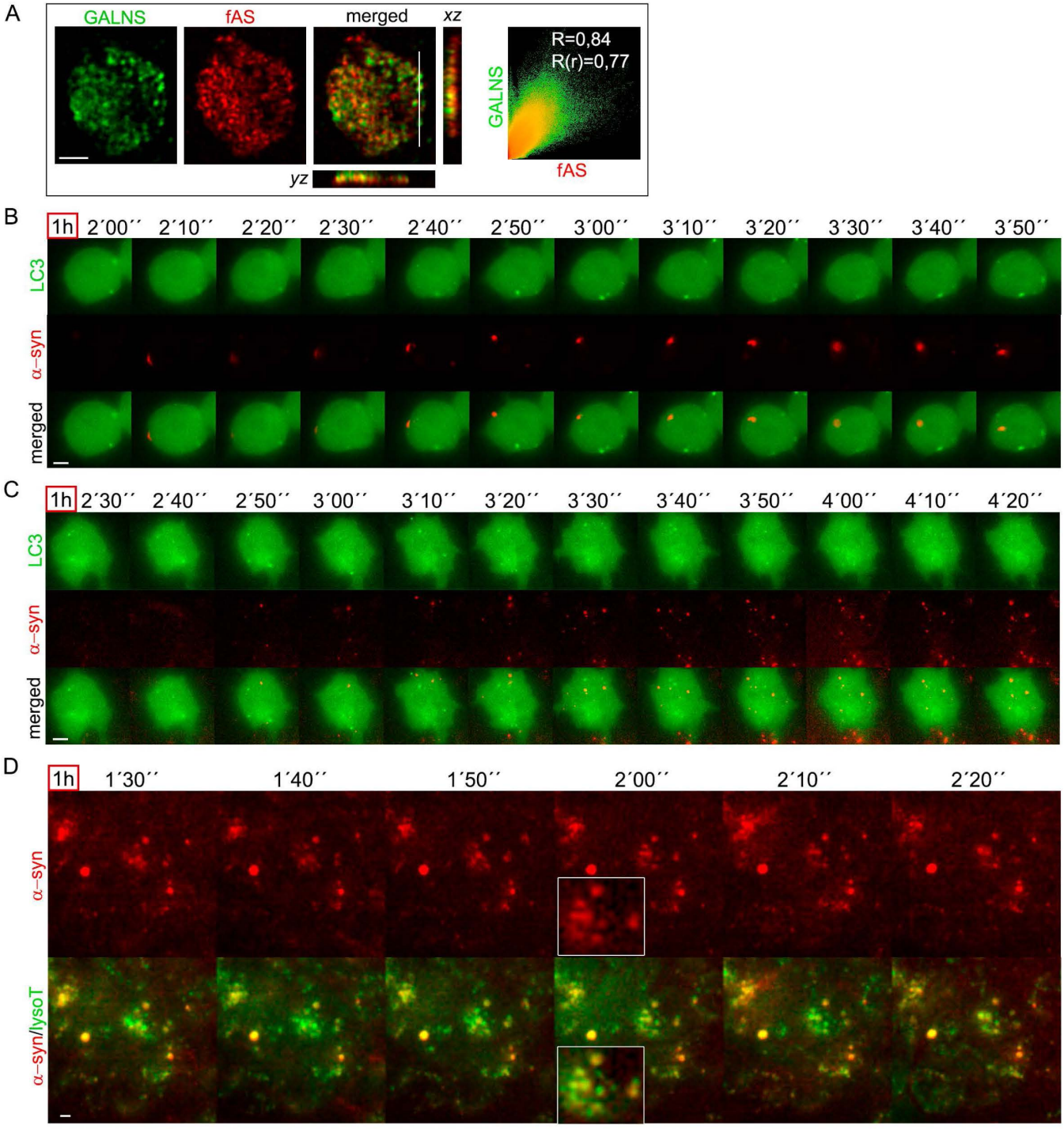

Figure S1.

Additional evaluation of lysosomal markers and autophagy dynamics of fAS-stimulated BV2 GFP-LC3 cells during early time points.

(A) Primary microglial cells were stimulated with fAS for 12h and co-localization between lysosomal specific marker GALNS and fAS was analysed by confocal microscopy. Pearson coefficient (R) and Overlap coefficient (R[r]) are listed. Scale bar, 5μm.

(B, C, D). BV2 GFP-LC3 (green) cells were stimulated with fAS (1uM, red) for 1h. Imaging started immediately after cellular stimulation and it was performed at 1 frame per 10 s during 1h, a selected interval within this sequence is shown. (C) shows fAS (red) and LysoTracker staining (green) of BV2 GFP-LC3 cells stimulated and imaged as described above. Of note that synuclein/LysoTracker co-localization is quickly observable after cellular internalization.

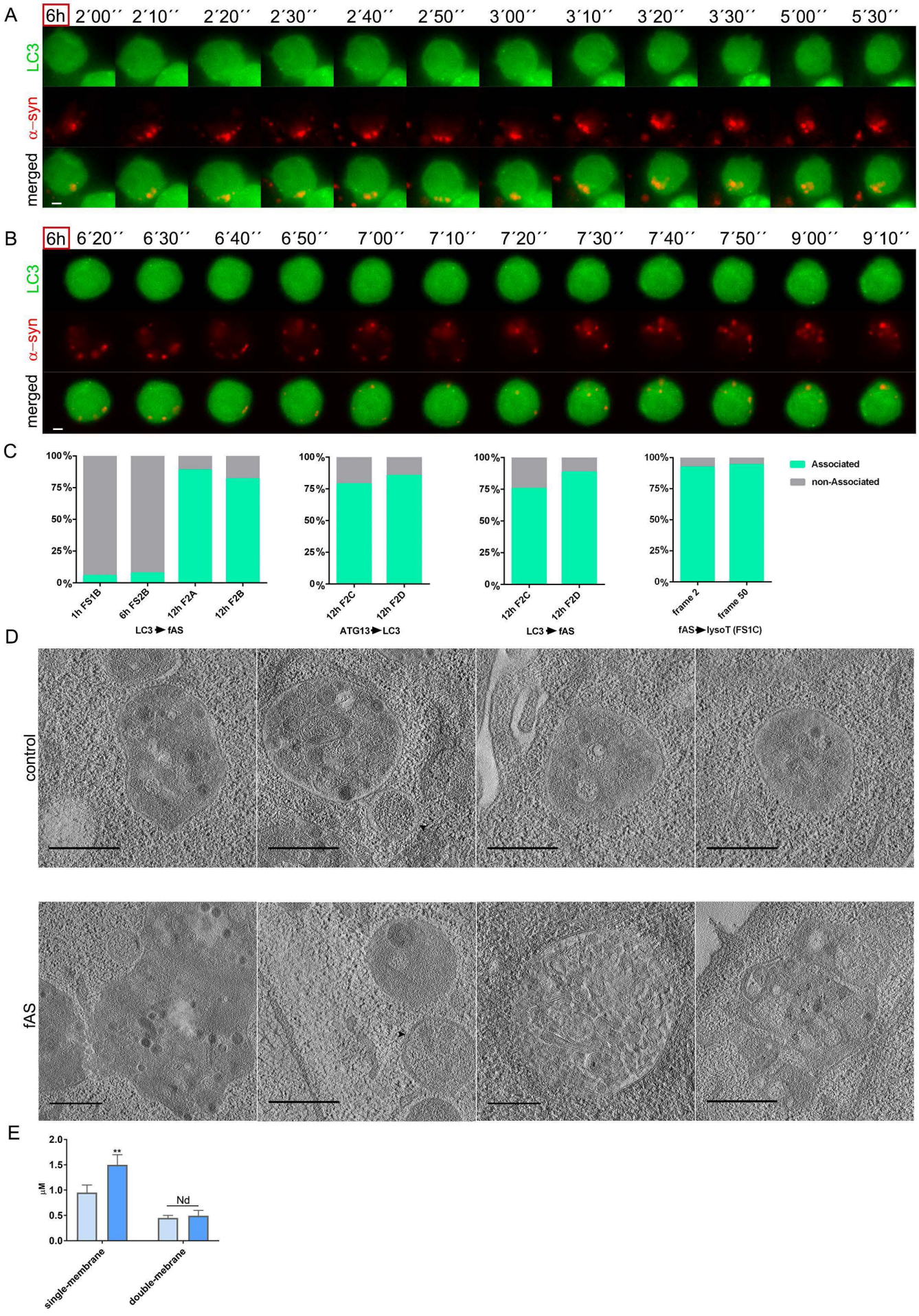

Figure S2.

Autophagy dynamics of fAS-stimulated BV2 GFP-LC3 cells during early time points (cont.) and comparison of single and double-membrane vesicles found in control and stimulated BV2 microglial cells.

A, B. BV2 GFP-LC3 (green) cells were stimulated with fAS (red) for 6h and imaged at 1 frame per 10 s during 1h, a selected interval within this sequence is shown. Scale bar, 2μm. (C) Values are percentages of association of LC3-positive vesicles with fAS; ATG13-positive vesicles with LC3; and fAS with LysoTracker-positive vesicles corresponding to analysis of time-lapse experiments from the indicated figures. (D) Representative images from EM tomograms of control and fAS-stimulated BV2 GFP-LC3 microglial cells showing different single and double membrane AV (scale bar, 500nm). (E) Graphs show the AV size quantification in both conditions. Results were analysed by one-way ANOVA followed by Post-Hoc Dunnet´s test; n = 30. Error bars represent SEM (*, $P < 0.05$; **, $P < 0.01$).

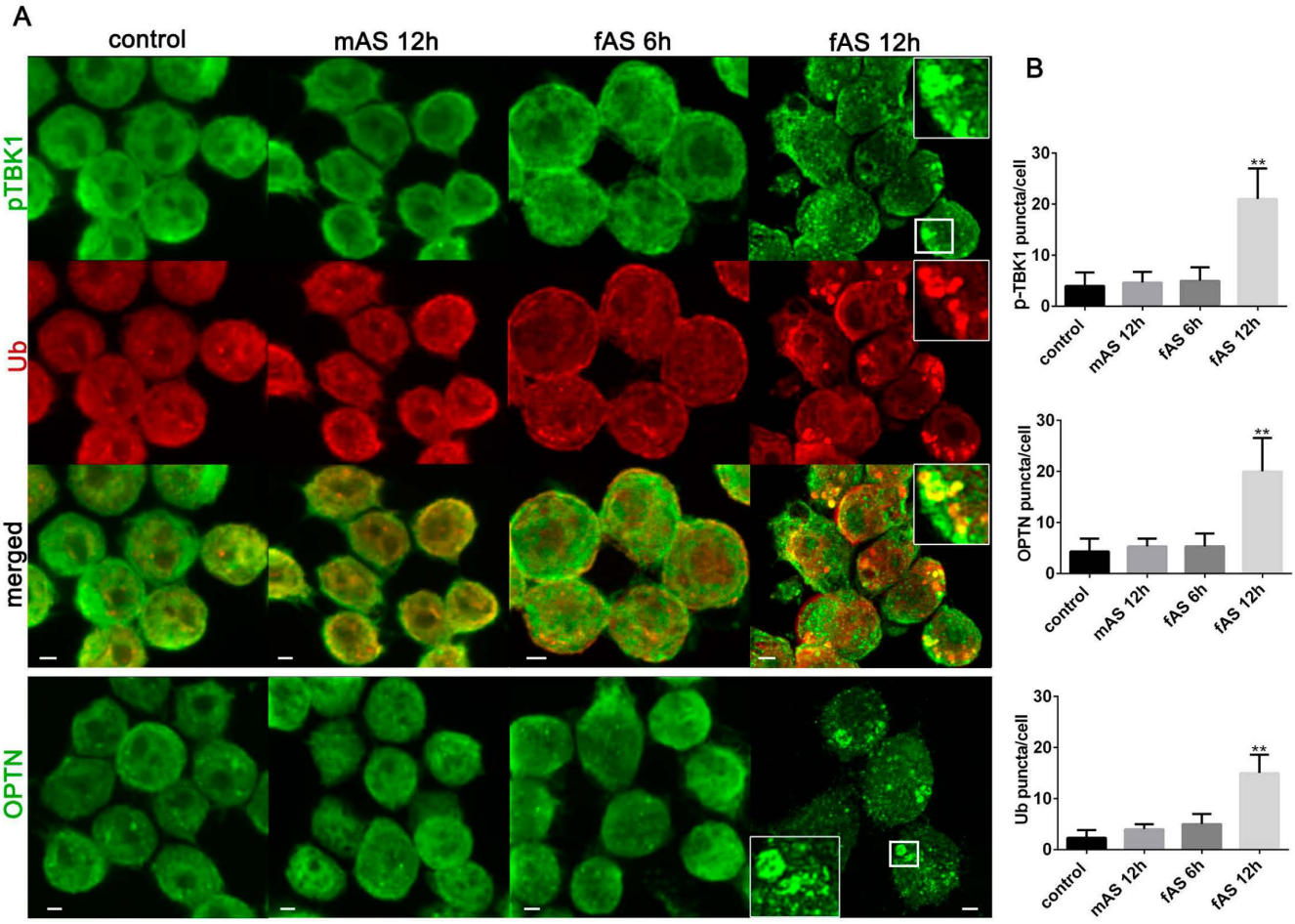

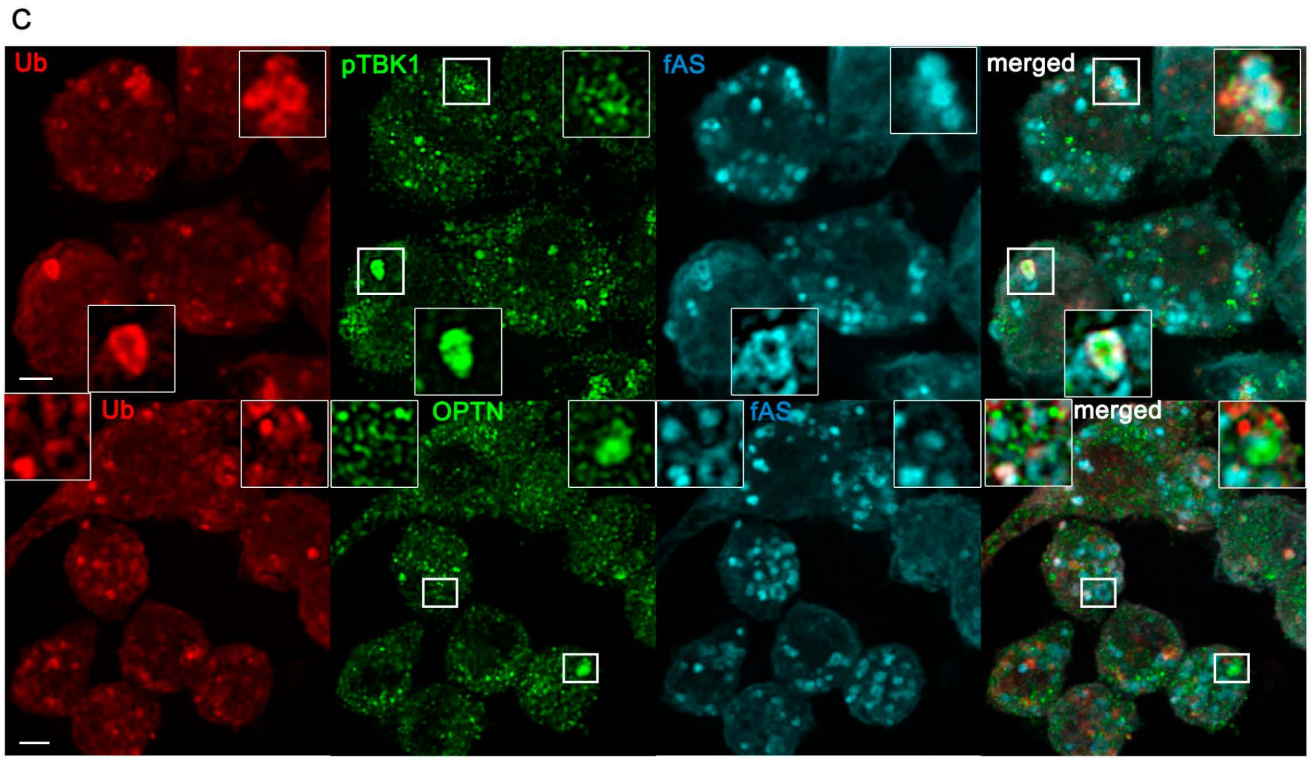

Figure S3.

OPTN and pTBK1 are recruited to lysosomal damage sites in fAS-stimulated microglial cells.

(A, B). BV2 cells were left untreated or stimulated with fibrillar (f) or monomeric (m) AS at the indicated time points. After that, cells were immunostained for pTBK1, ubiquitin (Ub) and OPTN. Puncta formation were determined using ImageJ particle counting plugin (B). Results were analysed by one-way ANOVA followed by Post-Hoc Dunnet´s test; n = 3. Error bars represent SEM (**, $P < 0.01$). (C) BV2 cells were stimulated with fAS (cyan) for 12h and were then fixed and stained for ubiquitin, pTBK1 and OPTN. Image crops shows magnification of the selected areas (white box).

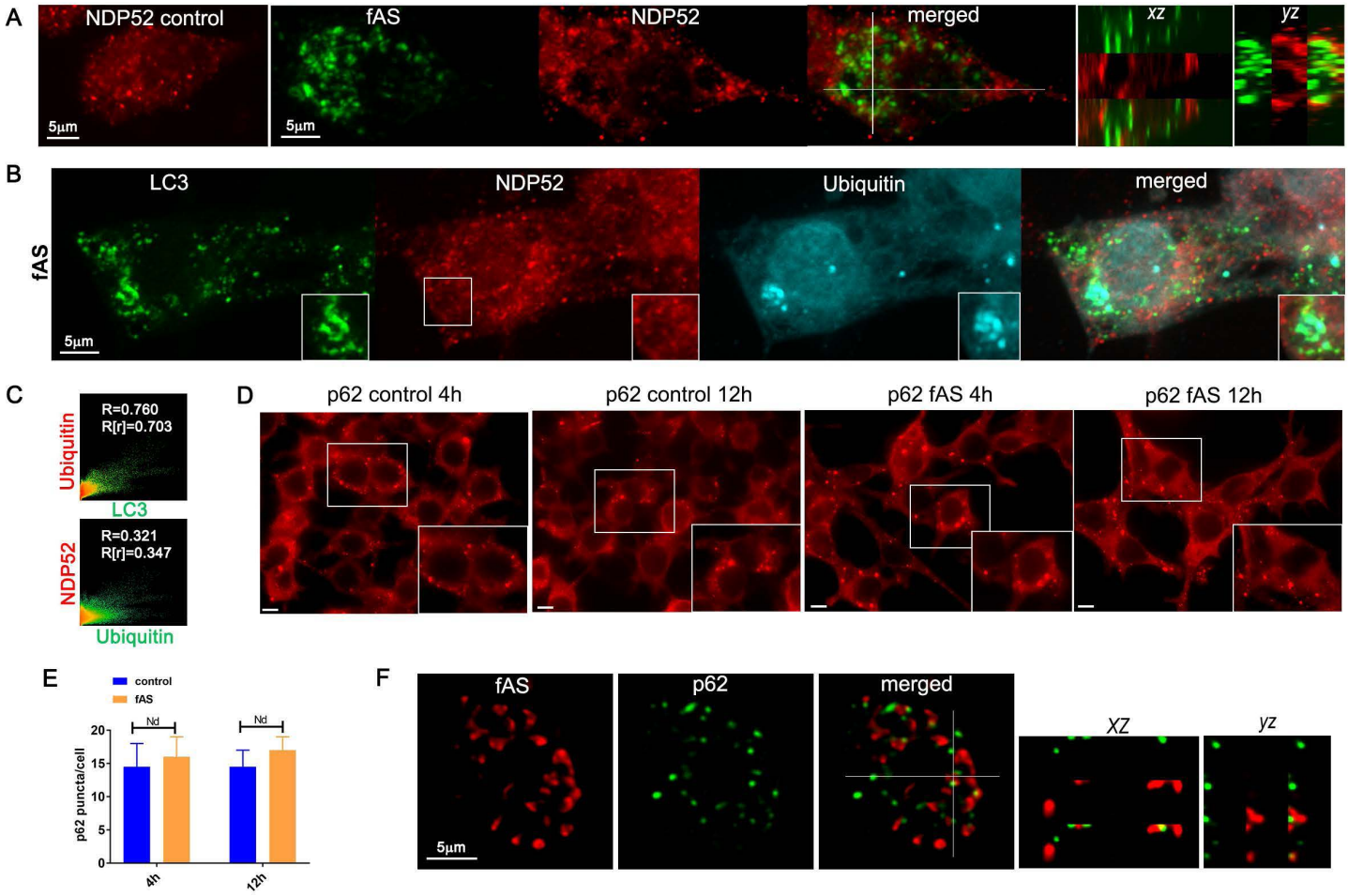

Figure S4.

NDP52 and p62 evaluation in fAS-stimulated microglial cells. (A) BV2 microglial cells were stimulated with fAS (green) for 12h. After that, cells were fixed and stained for NDP52 (red) and co-localization analysed with orthogonal views from z-stack confocal images. (B, C) fAS-stimulated BV2 GFP-LC3 cells were immunostained for NDP52 (red) and ubiquitin (cyan). (C) shows co-localization analysis of the selected area (white square) indicated in (B). Pearson coefficient (R) and Overlap coefficient (R[r]) are listed. (D, E) BV2 cells were stimulated with fAS (5µm) at the indicated time points or left untreated. Cells were then fixed and stained for p62 and p62-positive vesicles were quantified as shown in (E). (F) primary microglial cells were stimulated with fAS for 12h and stained for p62 (green). Co-localization was analysed with orthogonal views from z-stack confocal images after cellular deconvolution. A representative image sequence is shown (n=20).

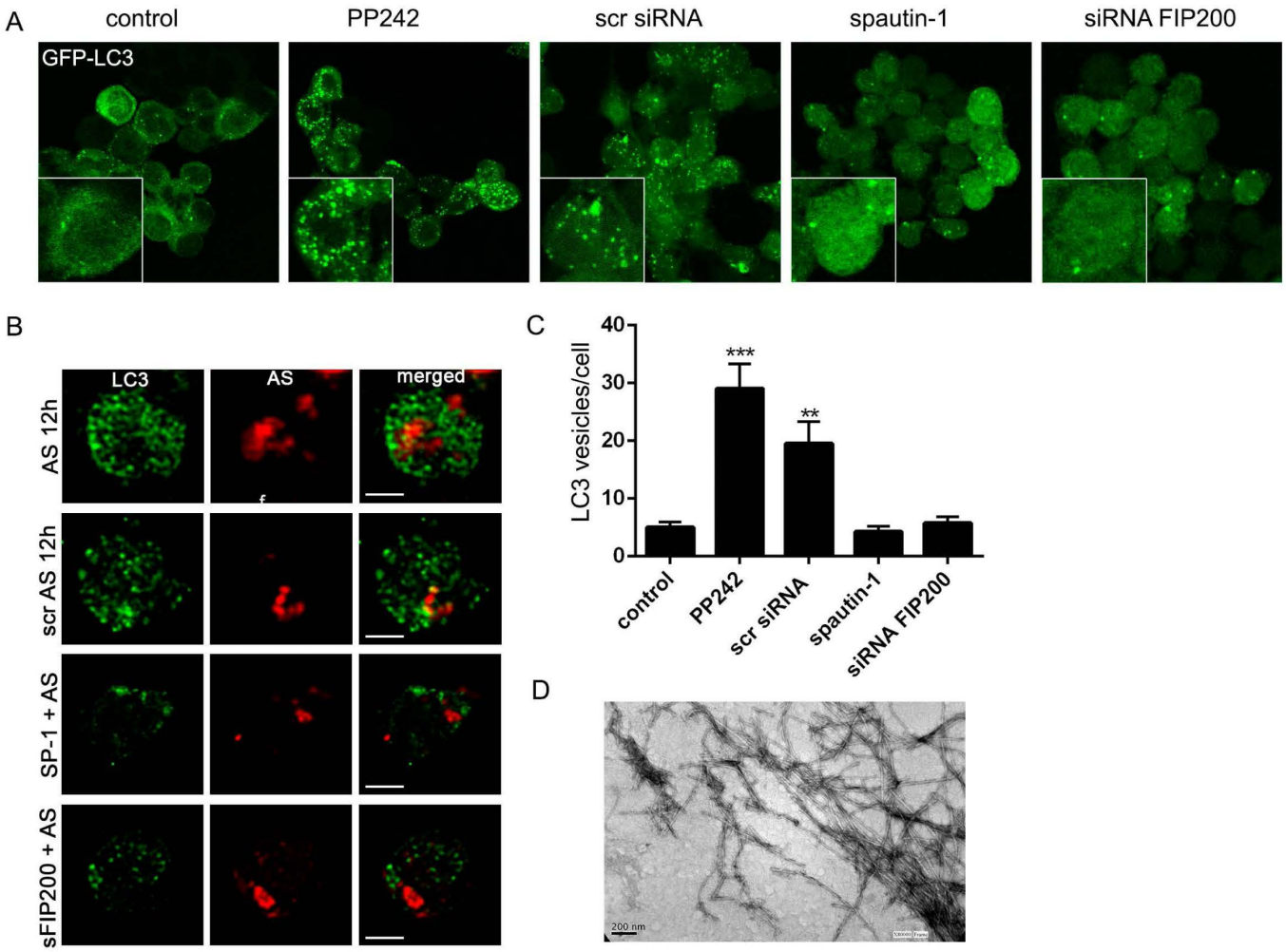

Figure S5.

Effects of spautin-1 and siRNAFIP200 on LC3 puncta induction.

(B) Representative Immunofluorescence images of BV2 GFP-LC3 cells treated with the mTOR inhibitor PP242 (1uM) for 3h in the presence or the absence of spautin-1 (10 μM) or siRNA FIP200. Spautin-1 and siRNA FIP200 were added 24h and 48 h before autophagy stimulation, respectively. (C) primary microglial cells were cultured in the presence or the absence of spautin-1 (10 μM) or siRNA FIP200 and stimulated with fAS (red, 5uM). After 12h, cells were immunostained for LC3 (green) and confocal images after cellular deconvolution are shown, scale bar, 5μm. (D) shows LC3 puncta quantification of the conditions indicated in (B). (E) TEM of fAS (scale bar, 200nm). Results were analysed by one-way ANOVA followed by Post-Hoc Dunnet´s test; n = 3. Error bars represent SEM (**, $P < 0.01$; ***, $P < 0.001$).

(Movies 1-9) Video files showing autophagy dynamics at different time points after fAS stimulation of BV2 microglial cells.

Movie 1

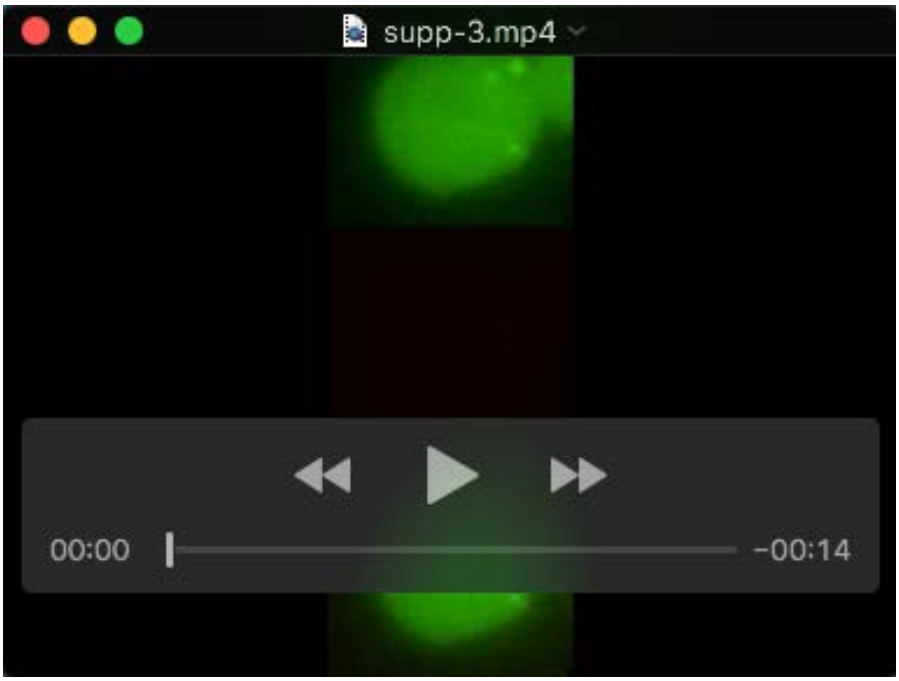

Movie 2

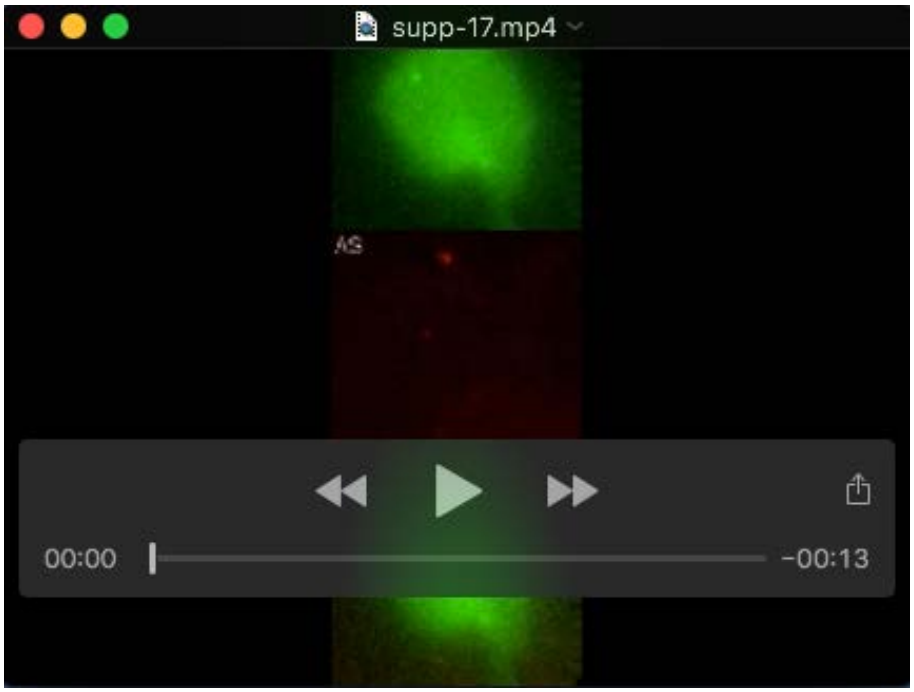

Journal of Cell Science • Supplementary information

Movie 3

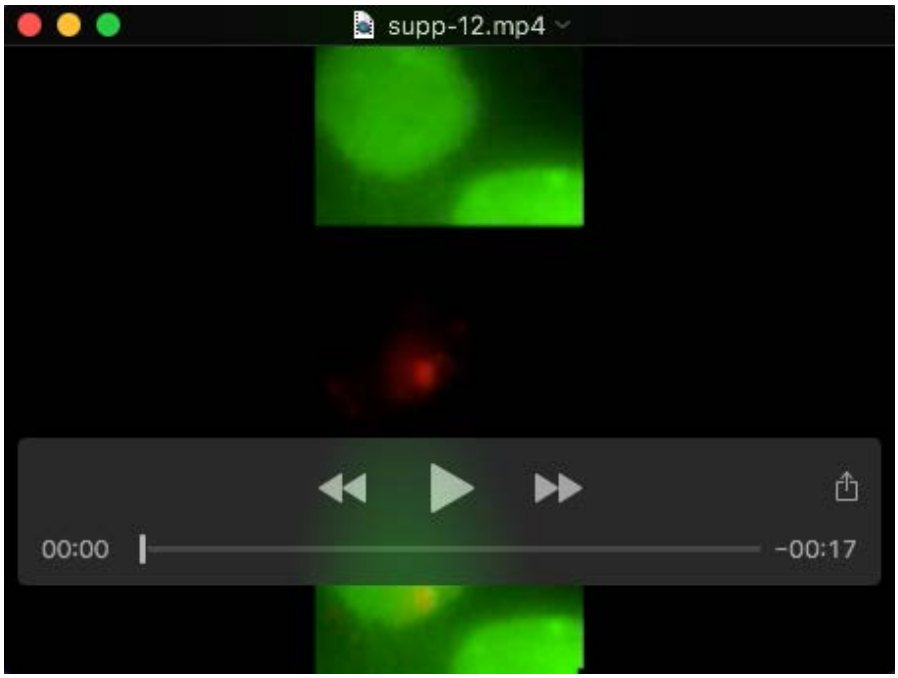

Movie 4

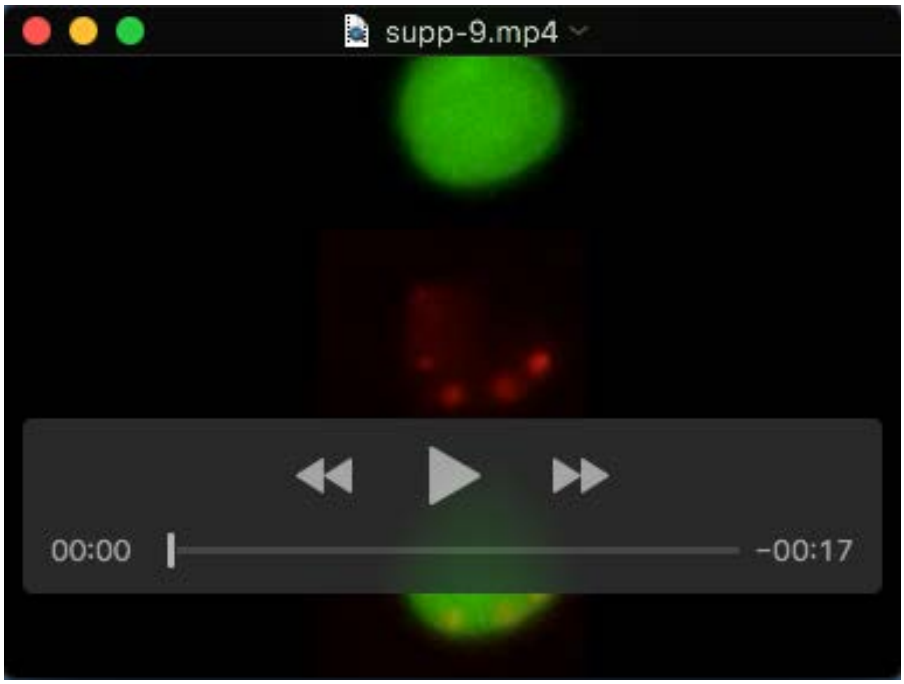

Movies 1, 2, 3 and 4. BV2 GFP-LC3 cells (green) were stimulated with fAS (red) and imaged immediately (Movie 1 and 2) or 6h after stimulation (Movie 3 and 4). Of note that no significant change in the dynamics of autophagy is detected over time, unlike long-term stimulation.

Movie 5

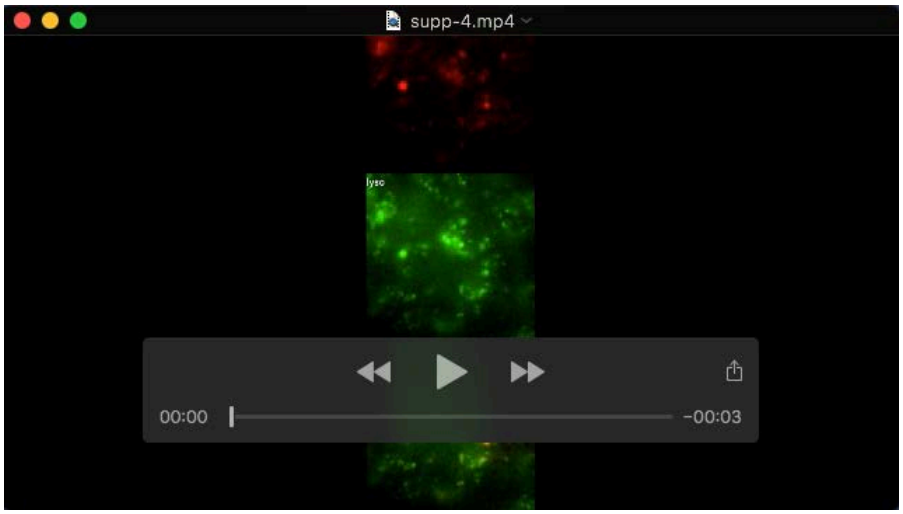

Movie 5. BV2 GFP-LC3 cells were stimulated with fAS (red) and imaged immediately after stimulation for 1h. LysoTracker (green) was used for lysosomal staining.

Movie 6

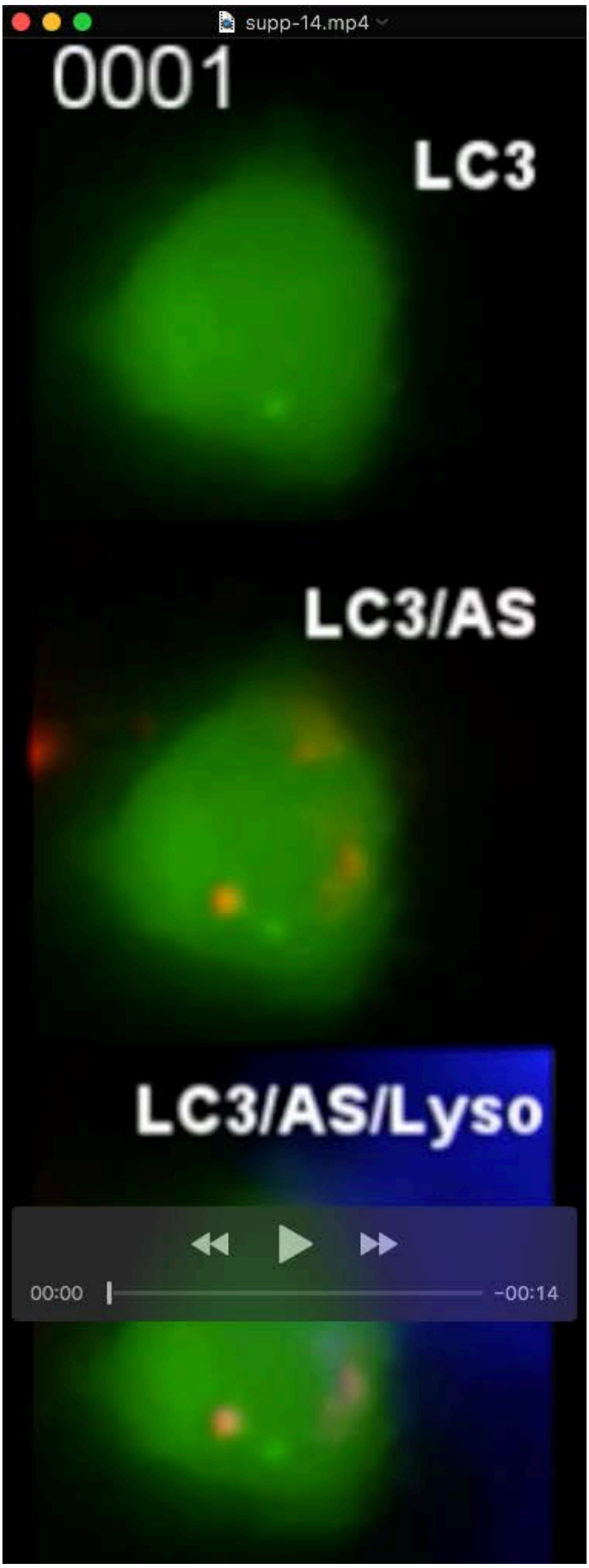

Journal of Cell Science • Supplementary information

Movie 7

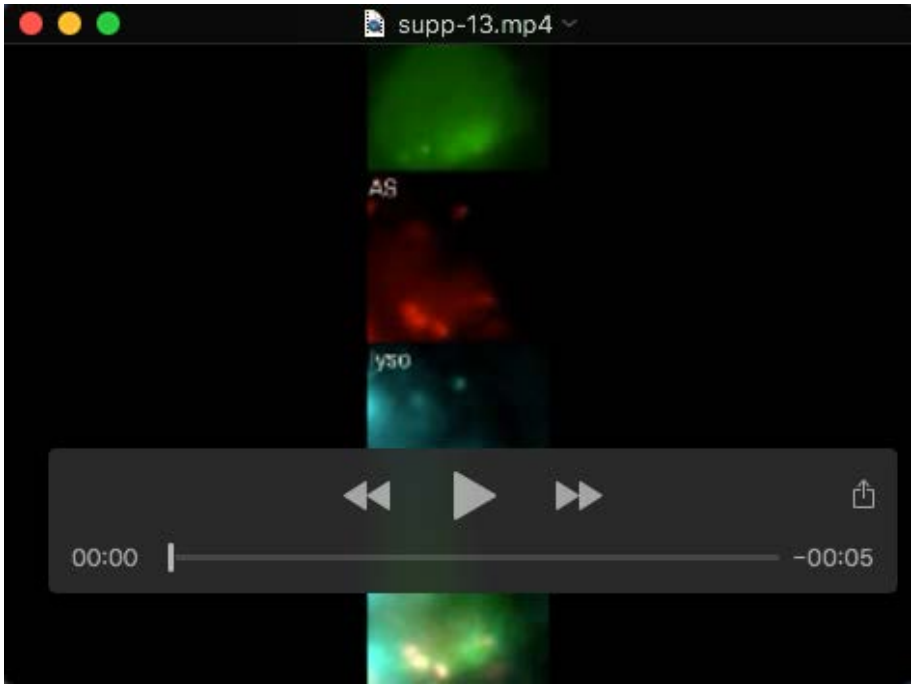

Movies 6 and 7. BV2 GFP-LC3 cells were stimulated with fAS for 12h and imaged at 1 frame per 10 s during 1h. Movie 6 and 7 correspond to the sequence shown in Fig. 2A and Fig. 2B, respectively. Of note that LC3 (green) forms a ring-like structure around fAS (red). LysoTracker (blue) was used for lysosomal staining.

Movie 8

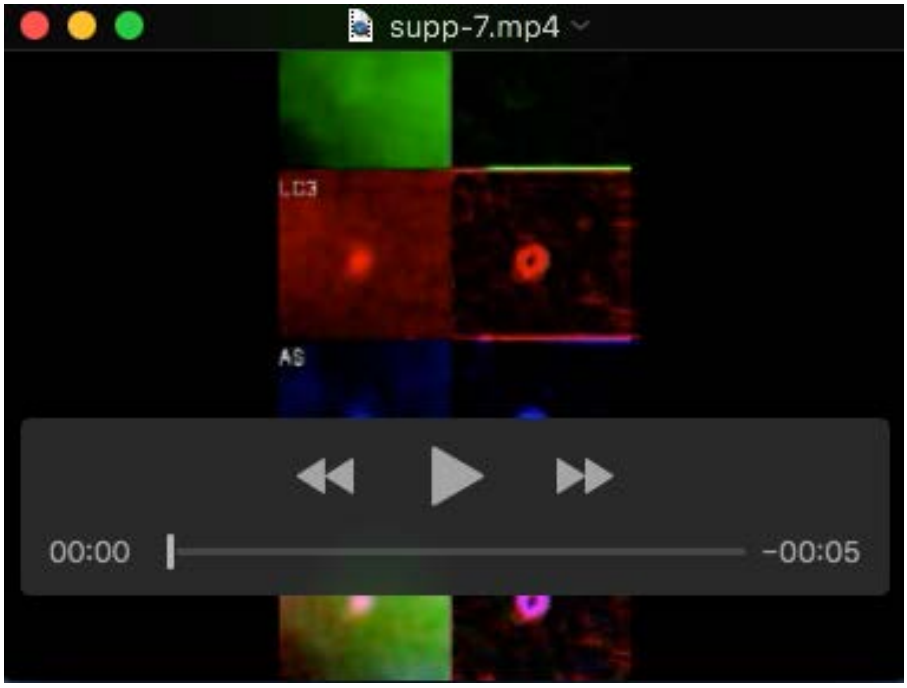

Movie 9

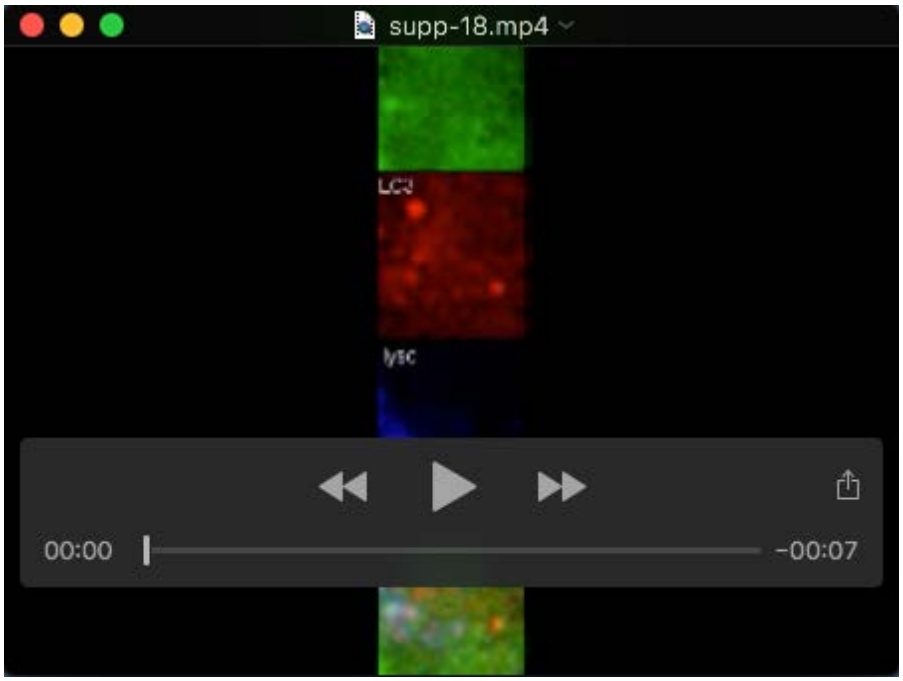

Movies 8 and 9. BV2 cells stably expressing ATG13 (green) were co-transfected with CFP-LC3 plasmid (red). Microglial cells were stimulated with fAS (blue) for 12h and imaged at 1 frame per 10 s during 1h. Movie 8 and 9 correspond to sequence shown in Fig. 2C and Fig. 2D, respectively. Of note that ATG13-positive structures mature into LC3-positive vesicles.

Movie 10

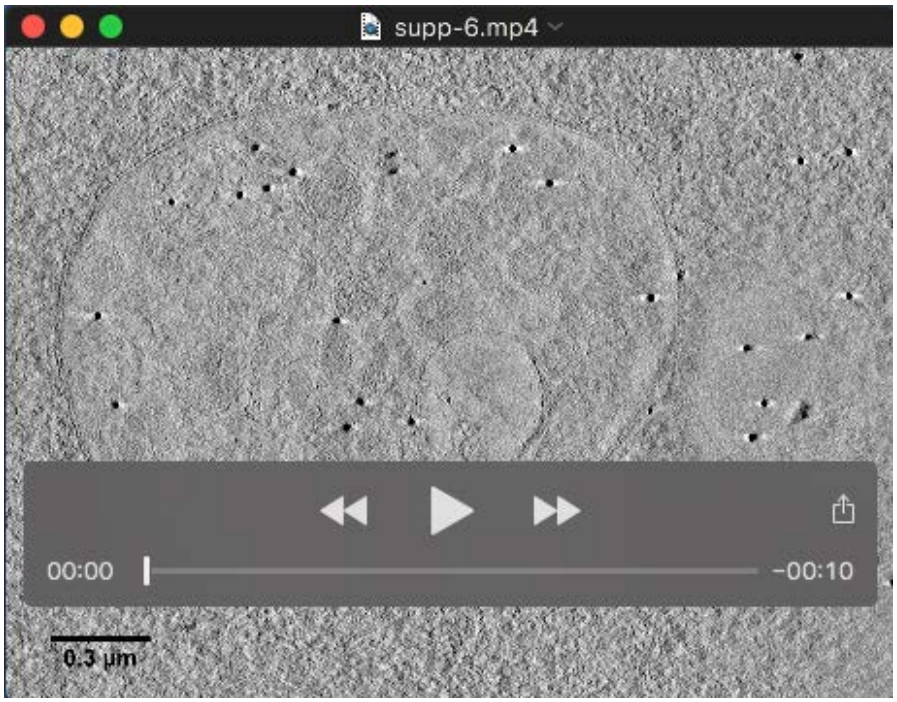

Movie 11

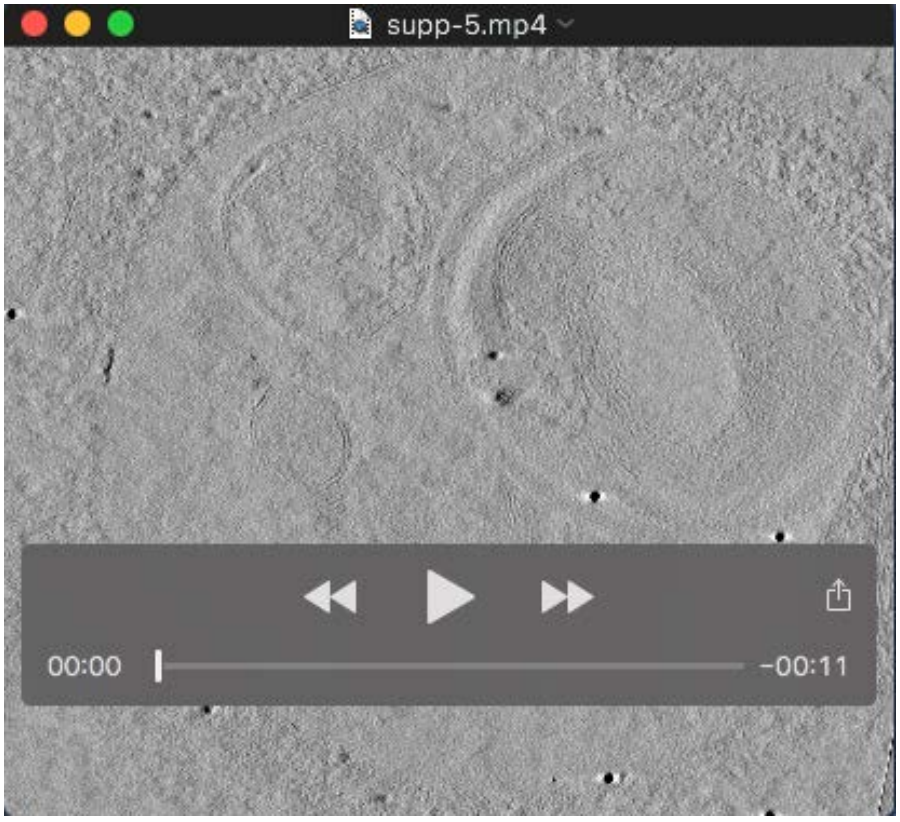

Journal of Cell Science • Supplementary information

Movie 12

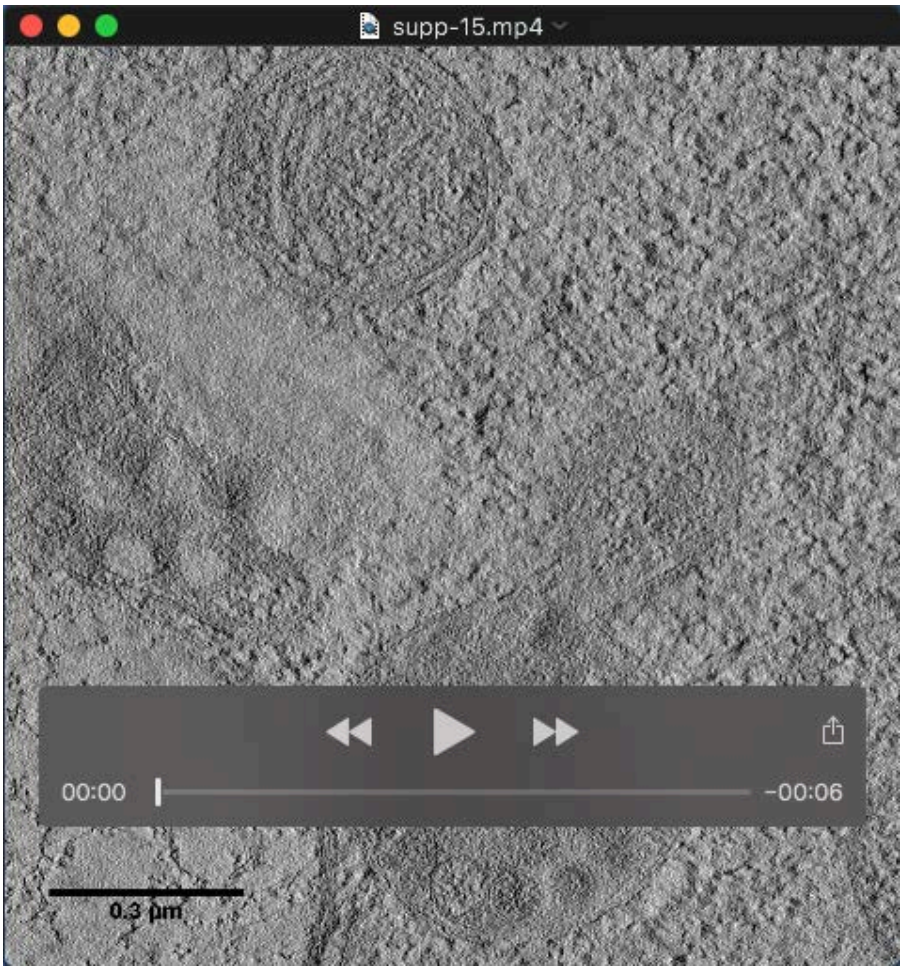

Movie 13

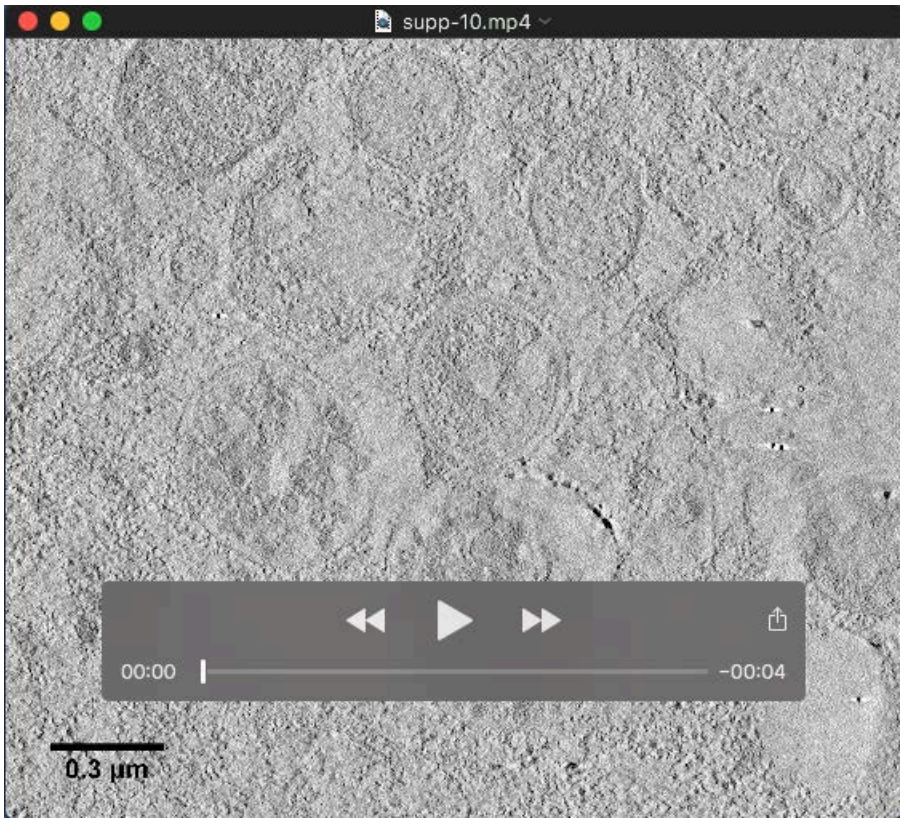

Journal of Cell Science • Supplementary information

Movies 10 – 13. EM tomograms from fAS-stimulated microglial cells.

EM high-magnification (20000X) tomograms corresponding to the images indicated as Fig. 3A (Movie 10), Fig. 3B (Movie 11), Fig. 3E (Movie 12) and Fig. 3G (Movie 13) are shown as video files. Of note, the presence of double membrane autophagosomes.

Movie 14

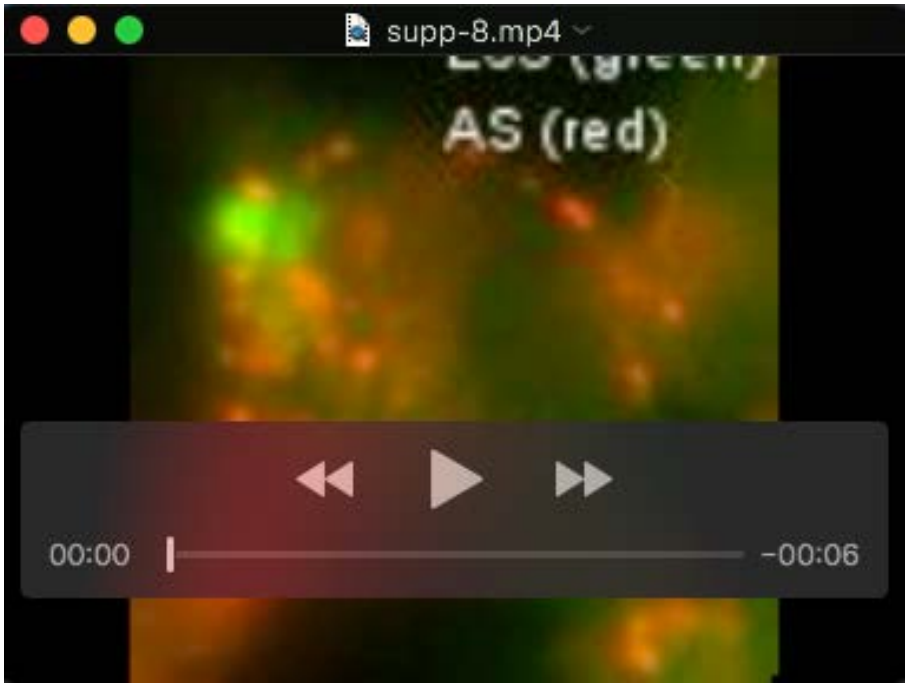

Movie 15

Movies 14, 15. Live imaging video file (Movie 14) and serial tomogram and 3D model (Movie 15) corresponding to Fig 4A and Fig. 4E, respectively. Tomograms of twenty consecutive 300nm sections were acquired at 9400X magnification and later aligned. Movie 15 shows a central double-membrane autophagosome containing several vesicles.

Movie 16

Movie 17

Movies 16 and 17. Live imaging video file (Movie 16) and serial tomogram and 3D model (Movie 17) corresponding to Fig. 4C and Fig. 4H, respectively. Movie 17 shows an inner autophagosome and multiple ER membranes surrounding it, suggesting it is an immature AV. Of note, an additional concentrical structure exhibiting a dense core is also exhibited.